

# Rothamsted Repository Download

## A - Papers appearing in refereed journals

Piovesana, M., Wood, A. K. M., Smith, D. P., Deery, M. J., Bayliss, R., Carrera, E., Napier, J. A., Kurup, S. and Matthes, M. C. 2023. A point mutation in the kinase domain of CRK10 leads to xylem vessel collapse and activates defence responses. *Journal of Experimental Botany*. p. erad80. <https://doi.org/10.1093/jxb/erad080>

The publisher's version can be accessed at:

- <https://doi.org/10.1093/jxb/erad080>

The output can be accessed at: <https://repository.rothamsted.ac.uk/item/98676/a-point-mutation-in-the-kinase-domain-of-crk10-leads-to-xylem-vessel-collapse-and-activates-defence-responses>.

© 3 March 2023, Please contact [library@rothamsted.ac.uk](mailto:library@rothamsted.ac.uk) for copyright queries.

1 **Short title:** Characterisation of a novel CRK10 mutant

2 **Author for contact detail:** michaela.matthes@rothamsted.ac.uk

3 **Title:** A point mutation in the kinase domain of CRK10 leads to xylem vessel collapse and  
4 activates defence responses

5

6 **Maiara Piovesana**<sup>1,2</sup>, **Ana K. M. Wood**<sup>3, §</sup>, **Daniel P. Smith**<sup>4</sup>, **Michael J. Deery**<sup>5</sup>, **Richard**

7 **Bayliss**<sup>6</sup>, **Esther Carrera**<sup>7</sup>, **Johnathan A. Napier**<sup>1</sup>, **Smita Kurup**<sup>1</sup>, **Michaela C. Matthes**<sup>1,\*</sup>,

8 <sup>1</sup> Department of Plant Sciences, Rothamsted Research, Harpenden, AL5 2JQ, United  
9 Kingdom.

10 <sup>2</sup> College of Life and Environmental Sciences, Streatham Campus, Exeter, EX4 4PY, United  
11 Kingdom.

12 <sup>3</sup> Department of Biointeractions and Crop Protection, Rothamsted Research, Harpenden, AL5  
13 2JQ, United Kingdom.

14 <sup>4</sup> Department of Computational and Analytical Sciences, Rothamsted Research, Harpenden,  
15 AL5 2JQ, United Kingdom

16 <sup>5</sup> Cambridge Centre for Proteomics, University of Cambridge, Cambridge, CB2 1QR, United  
17 Kingdom.

18 <sup>6</sup> School of Molecular and Cellular Biology, Faculty of Biological Sciences, University of  
19 Leeds, Leeds, LS2 9JT, United Kingdom.

20 <sup>7</sup> Instituto de Biología Molecular y Celular de Plantas, Universidad Politècnica de València,  
21 Valencia, 46022, Spain.

22 \* Author for communication: michaela.matthes@rothamsted.ac.uk

23 † Senior author

24 <sup>§</sup>Present address: Jealott's Hill International Research Centre, Syngenta, Bracknell, RG42  
25 6EY, United Kingdom.

26 **One sentence summary:** A mutated receptor-like kinase affects the xylem vasculature of  
27 roots and hypocotyls and induces constitutive defence responses to pathogens.

28

29 S. K. and M.C.M planned and designed the project. M.P. and M.C.M. performed most of the  
30 experiments. R.B. performed the kinase domain modelling. M.J.D. performed the protein  
31 mass spectrometry and analysis. E.C. provided the hormone data. A.K.M.W. assisted with the  
32 pathogen assays. D.P.S performed the RNA-Seq analysis. M.P, S.K., J.A.N. and M.C.M.  
33 wrote the manuscript.

34 The author responsible for distribution of materials integral to the findings presented in this  
35 article in accordance with the policy described in the Instructions for Authors  
36 (<https://academic.oup.com/plphys/pages/general-instructions>) is: Michaela C. Matthes  
37 ([michaela.matthes@rothamsted.ac.uk](mailto:michaela.matthes@rothamsted.ac.uk)).

38

## 39 **ABSTRACT**

40

41 Cysteine-rich receptor-like kinases (CRKs) are a large family of plasma membrane-  
42 bound receptors ubiquitous in higher plants. They are transcriptionally regulated by a wide  
43 variety of environmental cues and stresses, however their precise biological roles remain  
44 largely unknown. Here we report a novel mutant isolated for the CYSTEINE-RICH  
45 RECEPTOR-LIKE KINASE 10 (CRK10) of *Arabidopsis thaliana* which harbours the  
46 substitution of alanine 397 by a threonine in the  $\alpha$ C-helix of its kinase domain and which we  
47 registered as *crk10-A397T* in the community database. *In situ* phosphorylation assays with  
48 the His-tagged wild type (WT) and *crk10-A397T* versions of the CRK10 kinase domain  
49 revealed that both alleles are active kinases capable of auto-phosphorylation with the newly  
50 introduced threonine acting as an additional phosphorylation site in *crk10-A397T*.  
51 Phenotypically the mutant is a dwarf and the analysis of thin cross sections with light and  
52 transmission electron microscopy revealed that collapsed xylem vessels in roots and  
53 hypocotyls are very likely the cause for this reduction in stature. Transcriptomic analysis of  
54 WT and mutant hypocotyls revealed that predominantly biotic and abiotic stress-responsive  
55 genes are constitutively up-regulated in the mutant. Root-infection assays with the vascular

56 pathogen *Fusarium oxysporum* demonstrated that the *crk10-A397T* mutant has enhanced  
57 resistance to this pathogen compared to WT plants. Taken together our results suggest that  
58 *crk10-A397T* is a gain-of-function allele of *CRK10* and open up new avenues for the  
59 investigation of this elusive receptor-like kinase family.

60

## 61 INTRODUCTION

62

63 Plant growth and development is modulated by intrinsic growth regulators as well as  
64 by beneficial and adverse environmental cues. Factors regulating development and  
65 environmental and pathogenic signals are mostly recognised by receptor-like kinases (RLKs),  
66 membrane-localized receptors which perceive and transduce these signals inside plant cells to  
67 activate programmes directing appropriate responses. Similar to animal receptor tyrosine  
68 kinases (RTKs), these receptors consist of an extracellular domain which perceives specific  
69 ligands, a single pass transmembrane domain, and a cytoplasmic kinase domain which  
70 transduces the signal via phosphorylation of downstream target proteins in the cytoplasm in  
71 order to tailor a cellular response (Shiu & Bleecker, 2001; De Smet et al., 2009). Their highly  
72 variable extracellular domains are used to classify RLKs into subgroups, the largest of which  
73 (~200 genes in *Arabidopsis thaliana*) being characterised by leucine-rich repeats (LRR-  
74 RLKs) (Diévert & Clark, 2004). The well-studied brassinosteroid receptor  
75 BRASSINOSTEROID INSENSITIVE 1 (BRI1; AT4G39400) and the microbial pattern  
76 recognition receptors (PRR) FLAGELLIN SENSING 2 (FLS2; AT5G46330) and EF-TU  
77 RECEPTOR (EFR; AT5G20480) belong to this subgroup (Friedrichsen et al., 2000;  
78 Chinchilla et al., 2006; Zipfel et al., 2006).

79 Among the several subfamilies of RLKs found in plant genomes, the cysteine-rich  
80 receptor-like kinases (CRKs) is one of the largest with over 40 members in *Arabidopsis*. The  
81 signature motif for CRKs is the presence of, in most cases, two repeats of the DOMAIN OF  
82 UNKNOWN FUNCTION 26 (DUF26) in their extracellular domain, which contains three  
83 cysteine residues in the conserved configuration C-X8-C-X2-C (Chen, 2001). The functional  
84 significance of the DUF26 domain remains to be elucidated but was originally suggested to  
85 participate in ROS or redox sensing (Wrzaczek et al., 2010; Bourdais et al., 2015). However,  
86 more recent data obtained from the crystallographic analysis of the DUF26-containing  
87 ectodomain of the plasmodesmata localised proteins (PLDPs) PLDP5 and PLDP8 point

88 towards the involvement of the cysteine residues in forming disulfide bonds for the structural  
89 stabilisation of the protein, rather than redox sensing (Vaattovaara et al., 2019). The same  
90 study also revealed that the DUF26 domain shows strong structural similarity to fungal  
91 carbohydrate-binding lectins, which suggests that DUF26-containing proteins might  
92 constitute a group of carbohydrate-binding proteins in plants (Vaattovaara et al., 2019). That  
93 DUF26-containing proteins do interact with carbohydrates has been shown for the secreted  
94 antifungal protein from *Ginkgo biloba*, Ginkbilobin2 (Gnk2), which contains a single DUF26  
95 domain and acts as a mannose binding lectin (Miyakawa et al., 2009; Miyakawa et al., 2014),  
96 and for the secreted antifungal proteins AFP1 and AFP2 from maize, which contain tandem  
97 DUF26 domains also binding mannose (Ma et al., 2018). Ligands for the CRKs, however,  
98 still remain to be discovered.

99         Despite the prominence of the CRKs among the RLKs, very little is known about  
100 their specific functions and the regulation of downstream signalling events. Efforts to assign  
101 functions to CRKs involved a comprehensive analysis of a collection of T-DNA knockout  
102 lines for 41 CRKs of Arabidopsis, which suggested a role for several members in the fine-  
103 tuning of stress adaptation and plant development. Most knockout lines, however, did not  
104 display obvious phenotypes, as is expected for a large gene family due to redundancy  
105 amongst its members (Bourdais et al., 2015). Studies in Arabidopsis also revealed that several  
106 CRKs are transcriptionally regulated by a wide variety of biotic and abiotic factors such as  
107 ozone, ultraviolet light (UV), reactive oxygen species (ROS), the hormone salicylic acid (SA)  
108 and elicitation with pathogen-derived molecules (Czernic et al., 1999; Du & Chen, 2000;  
109 Ohtake et al., 2000; Wrzaczek et al., 2010). Functionally, CRKs belong to the RD subclass of  
110 Ser/Thr kinases (Vaattovaara et al., 2019), which typically carry a conserved arginine (R)  
111 immediately preceding the invariant aspartate (D) in subdomain VI required for catalytic  
112 activity and are in most cases activated through auto-phosphorylation of the activation loop  
113 (Nolen et al., 2004). Although the ability to auto-phosphorylate as well as to phosphorylate  
114 substrates *in situ* has been demonstrated for CRK2 and CRK7 (Idänheimo et al., 2014;  
115 Kimura et al., 2020), for example, detailed studies on the *in vivo* and *in vitro* role of  
116 phosphorylation sites are still outstanding for CRKs.

117         Gain-of-function mutations of a kinase are a valuable tool to study specific effects on cells  
118 and organisms, as in these instances the signalling cascade is initiated spontaneously without  
119 requiring the presence of an extracellular ligand. Although much is known about the

120 structure–function properties of eukaryotic kinases, predicting which point mutations will  
121 lead to a spontaneous activation of the signalling cascade is not straightforward and  
122 mutations are generally fortuitously isolated from mutagenic screens. In this study we  
123 describe the characterisation of such a gain-of-function mutant, *crk10-A397T*, obtained for  
124 the cysteine-rich receptor-like kinase CRK10 (AT4G23180) of *Arabidopsis*. This mutant  
125 contains a single amino acid substitution from alanine to threonine in the  $\alpha$ C-helix of the  
126 kinase domain of the protein, with the newly introduced Thr-397 acting as an additional *in*  
127 *situ* phosphorylation site. Defense responses are constitutively activated in the *crk10-A397T*  
128 mutant, as detected by transcriptome profiling, and resistance to a soil-borne vascular  
129 pathogen is significantly enhanced. In addition, we could link the dwarf phenotype of the  
130 mutant to the severe collapse of the xylem vessel elements which we showed to occur in the  
131 root and hypocotyl but, surprisingly, not in the shoot.

132

## 133 RESULTS

134

### 135 *crk10-A397T* is a semi-dominant mutant allele of CRK10

136 The *Arabidopsis thaliana* mutant characterised in this report was isolated in a forward  
137 genetic ethyl methanesulfonate (EMS) screen performed for an unrelated study. In brief, six  
138 rounds of backcrosses to the wild-type (WT) Col-0 parent were performed in order to clean  
139 the genetic background of the mutant before an in-depth characterisation. The homozygous  
140 mutant has a strong dwarf phenotype and observation of the segregating F2 progeny of the  
141 sixth backcross revealed the semi-dominant nature of the mutation, as WT, intermediate and  
142 dwarf phenotypes segregated according to a 1:2:1 ratio with heterozygous plants being  
143 clearly discernible (Supplemental Figure S1A;  $\chi^2_2 = 2.36$ ,  $p = 0.308$ ). In order to determine  
144 the underlying mutation responsible for the dwarf phenotype, whole genome sequencing was  
145 performed on bulk segregants derived from the sixth backcross. This returned a list of 15  
146 candidate genes containing point mutations in coding regions. We noticed that a substitution  
147 of G>A in the 4th exon of the *CYSTEINE-RICH RECEPTOR-LIKE KINASE 10* (*CRK10*;  
148 AT4G23180) lead to the substitution of alanine 397 by a threonine in the kinase domain of  
149 CRK10 (Supplemental Figure S1B). As we considered this receptor-like kinase to be the  
150 most likely candidate among the 15 identified genes, we tested whether the dwarf phenotype  
151 could be rescued by constitutive expression of the WT cDNA sequence of *CRK10* under the

152 control of the 35S promoter. All T1 transformants showed a WT phenotype (Supplemental  
153 Figure S1C), suggesting that we had identified the correct gene. To further confirm that the  
154 mutation in *CRK10* causes the dwarf morphology, we recreated the G>A substitution by *in*  
155 *vitro* mutagenesis in the cDNA sequence of *CRK10*, and introduced this ORF into a *crk10*  
156 KO background (*crk10-2*, SAIL\_427\_E09, characterisation of KO lines to follow) under the  
157 control of the 1 kb genomic region containing the putative native promoter of *CRK10*. A total  
158 of 25% of the recovered transformants were dwarfs, establishing a direct link between the  
159 dwarf phenotype and the mutant allele (Supplemental Figure S1D). Subsequently, we will  
160 refer to this mutant as *crk10-A397T*.

161

### 162 **The A397T substitution is localised in the $\alpha$ C-helix of the kinase domain of** 163 **CRK10**

164 According to the subdivision of eukaryotic kinase domains into 12 conserved  
165 subdomains (Hanks & Hunter, 1995), the A397T substitution is localised in subdomain III of  
166 the kinase domain of CRK10 (Figure 1A), which corresponds to the  $\alpha$ C-Helix motif in the  
167 three-dimensional structure of the protein. Homology modelling to the active kinase domain  
168 of the Arabidopsis BRASSINOSTEROID INSENSITIVE 1 (BRI1) positions Thr-397 at the  
169 C-terminal end of the helix, with its side chain likely to be exposed on the surface of the  
170 protein (Figure 1B).

171

### 172 **The cytoplasmic kinase domains of CRK10 and CRK10-A397T are active** 173 **kinases**

174 With CRKs being classified as Ser/Thr kinases, the substitution of Ala-397 by a  
175 threonine (A397T) in the CRK10 kinase domain could have introduced a potential additional  
176 phosphorylation site. We therefore wanted to determine whether WT and mutant CRK10 are  
177 enzymatically active kinases and if differences in their auto-phosphorylation pattern can be  
178 detected. We addressed this question by investigating the auto-phosphorylation activity of the  
179 cytoplasmic kinase domain of CRK10 *in situ* when expressed in *Escherichia coli* cells  
180 (Taylor et al., 2013). We purified the CRK10 WT cytoplasmic kinase domain as an N-  
181 terminal 6x His-tag fusion protein (His-CRK10kd<sup>WT</sup>) from *E. coli* cells, as well as its “dead”  
182 kinase counterpart which harboured the substitution of the essential aspartic acid 473 with an  
183 asparagine residue (His-CRK10kd<sup>WT-D473N</sup>). Following separation of the recombinant proteins

184 by SDS-PAGE and detection by anti-His immunoblotting, the dead kinase version His-  
185 CRK10kd<sup>WT-D473N</sup> migrated at the predicted molecular weight ( $M_r$ ) of 40 kDa, while the WT  
186 kinase version His-CRK10kd<sup>WT</sup> showed an electrophoretic mobility shift to larger  $M_r$ , known  
187 to occur for phosphorylated proteins (Wegener & Jones, 1984) (Figure 1C). In order to  
188 determine whether the A397T substitution in the CRK10 kinase domain affects its auto-  
189 phosphorylation activity, we generated constructs in which Ala-397 was replaced by  
190 threonine through *in vitro* mutagenesis (His-CRK10kd<sup>A397T</sup> and His-CRK10kd<sup>A397T-D473N</sup>).  
191 Although the dead kinase version His-CRK10kd<sup>A397T-D473N</sup> migrated at the same  $M_r$  as His-  
192 CRK10kd<sup>WT-D473N</sup> on SDS-PAGE gels, the mobility shift of the His-CRK10kd<sup>A397T</sup> was  
193 increased when compared to the one observed for His-CRK10kd<sup>WT</sup> (Figure 1C), suggesting  
194 additional sites were phosphorylated in His-CRK10kd<sup>A397T</sup>. In order to confirm that the  
195 electrophoretic mobility shift was due to the presence of phosphorylated residues, the purified  
196 recombinant proteins were treated with  $\lambda$ -phosphatase prior to separation by SDS-PAGE.  
197 Irrespective of the treatments, the dead kinase versions CRK10kd<sup>WT-D473N</sup> and His-  
198 CRK10kd<sup>A397T-D473N</sup> migrated at the predicted  $M_r$  as confirmed by SDS-PAGE and anti-His  
199 immunoblotting (Figure 1D). However,  $\lambda$ -phosphatase treatment of His-CRK10kd<sup>WT</sup> and His-  
200 CRK10kd<sup>A397T</sup> resulted in a clearly detectable shift to a lower  $M_r$ , consistent with the auto-  
201 phosphorylation of recombinant His-CRK10kd<sup>WT</sup> and His-CRK10kd<sup>A397T</sup> as being  
202 responsible for their electrophoretic mobility shift. Taken together, these results confirm that  
203 both His-CRK10kd<sup>WT</sup> and His-CRK10kd<sup>A397T</sup> are active kinases capable of auto-  
204 phosphorylation. Furthermore, the increased mobility shift of His-CRK10kd<sup>A397T</sup> compared to  
205 His-CRK10kd<sup>WT</sup> suggested the presence of additional phosphorylation sites in His-  
206 CRK10kd<sup>A397T</sup>.

207

208 **The kinase domain of CRK10 auto-phosphorylates highly conserved residues in**  
209 **the activation loop and Thr-397 is an additional phosphorylation site in His-**  
210 **CRK10kd<sup>A397T</sup>**

211 We next proceeded to identify which sites in the kinase domain of CRK10 are being  
212 phosphorylated by subjecting tryptic peptides of His-CRK10kd<sup>WT</sup> and His-CRK10kd<sup>A397T</sup> to  
213 analysis by liquid chromatography-tandem mass spectrometry analysis (LC-MS/MS). The  
214 Mascot probability-based algorithm was used to confirm the peptides match to the CRK10  
215 kinase domain sequence. Individual MS/MS spectra were inspected for confirmation of

216 phosphorylation sites, which led to the unambiguous identification of Thr-340, Tyr-363, Thr-  
217 507, Ser-508, Tyr-514, Thr-625, Ser-662 and Thr-664 as phosphosites in both His-  
218 CRK10kd<sup>WT</sup> and His-CRK10kd<sup>A397T</sup> proteins (Figure 1E). Interestingly, Thr-507, Ser-508,  
219 and Tyr-514 align to conserved phosphorylation sites in the activation loop of several RLKs,  
220 known to be essential for the activation of RD kinases (Supplemental Figure S2).  
221 Phosphorylated residues were also detected in the juxta-membrane region (Thr-340) as well  
222 as in the C-terminal tail of CRK10 (Thr-625, Ser-662, and Thr-664), which are predicted to  
223 act as regulatory sites for interaction with binding partners. In addition, the identification of  
224 two phosphorylated tyrosine residues (Tyr-363 and Tyr-514) classifies CRK10 as dual  
225 specificity kinase and constitutes the first instance in which such activity has been reported  
226 for a CRK. Interestingly, Thr-397 itself was identified as a phosphorylation site in the His-  
227 CRK10kd<sup>A397T</sup> kinase domain *in situ* (Figure 1F), however, whether Thr-397 also acts as a  
228 phosphorylation site *in vivo* remains to be determined.

229

### 230 **The *crk10-A397T* mutant is a dwarf**

231 WT Col-0 and *crk10-A397T* plants were phenotypically characterised for the duration  
232 of one life cycle. Although germination rate and establishment of seedlings is accelerated in  
233 the mutant (Supplemental Figure S3), one week after sowing these differences are no longer  
234 apparent. No other obvious differences in growth were observed between WT and *crk10-*  
235 *A397T* seedlings until between weeks two and three, when leaf expansion becomes restricted  
236 in the *crk10-A397T* mutant as small, dark green leaves are formed, and a reduction of more  
237 than 70% in rosette size is observed at four weeks after sowing compared to the WT (Figure  
238 2A-G; Supplemental Figure S4A). Despite the dwarf phenotype displayed during vegetative  
239 growth, the onset of flowering occurs simultaneously in *crk10-A397T* mutant and WT plants,  
240 although the shoot apical meristem is frequently aborted in the mutant (Supplemental Figure  
241 S4B), and the main inflorescence remains stunted (Figure 2H). At later stages, mutant plants  
242 develop numerous lateral inflorescences with smaller, stunted siliques filled with viable seeds  
243 which are in general larger than those of WT plants (Figure 2-IK).

244

### 245 **The *crk10-A397T* mutant has collapsed xylem vessels in roots and hypocotyls**

246 Dwarfism in plants is often caused by defects in the vascular system. To investigate  
247 whether the vasculature of the *crk10-A397T* mutant develops normally, we prepared

248 transverse cross sections of resin-embedded hypocotyl, root and stem samples of 5-week-old  
249 plants. The sections were stained with potassium permanganate, a lignin-specific dye which  
250 allows the observation of lignified xylem vessels and fibres. Imaging of the cross sections  
251 revealed that xylem vessels in the root and hypocotyl of the mutant plants are severely  
252 collapsed, whereas the vasculature in the stem is not morphologically altered (Figure 3A-F).  
253 Interestingly, the collapsed xylem vessels displayed darker brown staining in response to the  
254 dye compared to their WT counterparts, which suggests that their secondary cell walls are  
255 more heavily lignified (Figure 3G-H). This hypothesis was reinforced by the visualization of  
256 auto-fluorescence of lignin of these cells using confocal microscopy, as the xylem vessels in  
257 the mutant hypocotyl consistently exhibited a more intense auto-fluorescence signal  
258 compared to the WT (Figure 3I-J). Transmission electron microscopy (TEM) was used to  
259 investigate potential defects in the ultrastructure of the secondary cell wall of the collapsed  
260 xylem vessels in 3-week-old hypocotyls, but no differences were observed in electron density  
261 and general appearance of the cell walls compared to that of intact vessels in the WT  
262 (Supplemental Figure S5).

263 To understand the progression of the phenotype, a developmental time series of  
264 hypocotyl cross sections spanning weeks one to five after sowing was analysed. Cross  
265 sections of one- and two-week-old hypocotyls revealed the disorganization of xylem vessels  
266 in *crk10-A397T* plants at early developmental stages, as they do not proceed to form the  
267 typical radial patterning observed in the hypocotyl vasculature of WT plants (Supplemental  
268 Figure S6A-D). At three weeks of age, the first deformed and collapsed xylem vessels  
269 become apparent in the mutant hypocotyls, a phenotype which is even more severe in 4-  
270 week-old plants (Supplemental Figure S6E-H). At 5 weeks of age, following the onset of  
271 flowering, cross sections revealed the absence of fully differentiated xylem fibres in the  
272 hypocotyl of the *crk10-A397T* plants, in contrast to the WT (Supplemental Figure S6I-L).  
273 Differentiation of xylary fibres in *Arabidopsis* hypocotyls is tightly associated with the  
274 switch to growth phase II of xylem development, which is triggered by the transition to  
275 flowering. We conclude that this switch is delayed in the *crk10-A397T* plants, despite  
276 flowering occurring simultaneously to WT plants.

277

278 **Loss of function or overexpression of *CRK10* does not cause a phenotype in**  
279 ***Arabidopsis***

280 In order to investigate whether increased levels of *CRK10* expression has observable  
281 phenotypic effects, we introduced a construct carrying the WT cDNA of *CRK10* under the  
282 control of the constitutive 35S promoter in WT *Arabidopsis* plants. Two independent  
283 homozygous lines were generated and selected for further analysis (*CRK10* OE-1 and OE-2).  
284 Compared to WT, qPCR performed on 4-week-old leaves detected a *CRK10* transcript  
285 increase of 15 and 6 times for *CRK10* OE-1 and OE-2, respectively, although growth and  
286 development were not altered (Supplemental Figure S7). In order to investigate whether the  
287 absence of the *CRK10* transcript affects the phenotype of *Arabidopsis* plants, two  
288 homozygous T-DNA knockout lines for the *CRK10* gene were isolated, *crk10-2*  
289 (SAIL\_427\_E09) and *crk10-4* (SALK\_116653). Quantification of *CRK10* transcript levels  
290 from leaves of 4-week-old plants by qPCR confirmed that *crk10-2* and *crk10-4* are a  
291 knockout and knockdown line of *CRK10*, respectively, however growth and development of  
292 both lines were indistinguishable from WT plants (Supplemental Figure S8). Cross sections  
293 of hypocotyls of 4-week-old *crk10-2* and *CRK10* OE-1 plants were imaged to rule out the  
294 presence of collapsed xylem vessels (Supplemental Figure S9). Lines *CRK10* OE-1 and  
295 *crk10-2* were used for the pathogen assays which are described in a subsequent section.

296

### 297 ***CRK10* is expressed in close association with vascular tissues and the protein** 298 **localises to the plasma membrane**

299 Tissue specific expression of *CRK10* was determined by placing the reporter  $\beta$ -  
300 *glucuronidase* under the control of the 1 kb genomic sequence containing the putative  
301 promoter of *CRK10* (*CRK10*<sub>Pro</sub>:GUS). *GUS* expression was detected in the vasculature of the  
302 roots, cotyledons, petioles, leaves, hypocotyls and inflorescence stem (Figure 4A-B;  
303 Supplemental Figure S10A-D). In hypocotyls of 2-week-old seedlings, expression was  
304 localised to differentiating xylem vessels and parenchyma cells surrounding the vessel  
305 elements (Figure 4B). The presence of the *CRK10* transcript in hypocotyls and inflorescence  
306 stems of 3- and 6-week-old WT and *crk10-A397T* mutant plants, respectively, was confirmed  
307 by qPCR (Supplemental Figure S10E).

308 Subcellular localisation of *CRK10* was determined by analysing lines expressing a  
309 construct carrying the C-terminal translational fusion of *CRK10* with the fluorescent protein  
310 mCherry under the control of the constitutive 35S promoter (*35S:CRK10-mCherry*). Both  
311 transient expression of the construct in *N. benthamiana* leaves and stable expression in

312 transgenic *Arabidopsis* plants indicated that the fusion protein localises to the plasma  
313 membrane (Supplemental Figure S10F; Figure 4C). The presence of Hechtian strands,  
314 characteristic of the retracting plasma membrane from the cell wall following plasmolysis  
315 (Oparka, 1994), further confirmed this subcellular localisation of the protein (Figure 4D).  
316 Therefore, we conclude *CRK10* is expressed in close association with vascular tissues of  
317 below and aboveground organs, and the protein localises to the plasma membrane of plant  
318 cells.

### 319 **Collapsed xylem vessels in the root and hypocotyl are responsible for the dwarf** 320 **phenotype of the *crk10-A397T* mutant**

321 Although *CRK10* is expressed in tissues associated with vasculature in the stem,  
322 hypocotyl and roots, as demonstrated by *CRK10*<sub>Pro</sub>:*GUS* analysis, it is intriguing that in the  
323 *crk10-A397T* plants xylem vessel collapse occurs only in roots and hypocotyls. To investigate  
324 if the dwarf phenotype is solely due to the defects of the below ground tissues, or whether it  
325 is a “whole-plant” response, we performed a micrografting experiment (Turnbull et al.,  
326 2002). *In vitro* grown 4-day-old seedlings were used to generate combinations of WT  
327 rootstocks and *crk10-A397T* scions (WT/*crk10-A397T*) and vice-versa (*crk10-A397T*/WT), as  
328 well as self-grafted plants as controls (WT/WT and *crk10-A397T/crk10-A397T*). Phenotypic  
329 assessment of successful grafts revealed that a WT scion grafted onto a *crk10-A397T*  
330 rootstock develops the characteristic dwarf phenotype of the mutant, whereas a mutant scion  
331 develops into a WT-like plant when grafted onto a WT rootstock (Figure 5). Our observations  
332 show that the root and hypocotyl system of the *crk10-A397T* plants are responsible for their  
333 dwarf phenotype, which is likely due to the presence of collapsed xylem vessels in these  
334 tissues.

335

### 336 **The hypocotyl transcriptome of *crk10-A397T* carries the signature of a plant** 337 **responding to stress**

338 The effect of the *crk10-A397T* mutation on the transcriptome was analysed by RNA-  
339 Seq. Total RNA was isolated from 15-, 21- and 35-day-old WT and mutant hypocotyls,  
340 which corresponds to the time points used for morphological analysis. Principal component  
341 analysis (PCA) showed good clustering of replicates according to genotypes and  
342 developmental time points (Supplemental Figure S11A). Following normalization and  
343 statistical analysis of the sequencing results ( $q \leq 0.05$ ;  $\log_2$  fold change threshold of  $\pm 1$ ), we

344 obtained 523 (15 days), 1836 (21 days) and 913 (35 days) differentially expressed genes  
345 (DEG), of which 274 were common to all time points. These DEGs were selected as the core  
346 set and taken forward for analysis (Figure 6A; Supplemental Figure S11B; Supplemental  
347 Tables S1-S4). Comparison to public datasets using the GENEVESTIGATOR® Signature  
348 tool (Hruz et al., 2008) revealed that the transcriptome signature of the *crk10-A397T* mutant  
349 was most similar to Arabidopsis plants challenged by fungal and bacterial pathogens  
350 (*Sclerotinia sclerotorum*, *Plectosphaerella cucumerina* and *Pseudomonas syringae*) and  
351 exposed to abiotic stress (treatment with fenclorim and sulfometuron methyl) (Figure 6C).  
352 Equally, Gene Ontology (GO) enrichment analysis of the up-regulated genes within the core  
353 set (246 genes) with AgriGO v.20 (Tian et al., 2017; False Discovery Rate < 0.05) revealed  
354 that terms associated with the biological functions “Defense response” (GO:0006952;  
355 p=2.30E-26), “Response to stimulus” (GO:0050896; p=1.40E-24) and “Response to stress”  
356 (GO:0006950; p=2.00E-24) are significantly overrepresented (Figure 6B; Supplemental  
357 Tables S5-S6). In accordance with the whole transcriptome data, marker genes indicative for  
358 the activation of the salicylic acid (SA)- and jasmonic acid (JA)-regulated defense pathways,  
359 such as pathogenesis-related and camalexin biosynthetic genes (Uknes et al., 1992; Thomma  
360 et al., 1998; Ahuja et al., 2012), are highly up-regulated in the *crk10-A397T* mutant  
361 (Supplemental Table S7). Transcription factors belonging to the WRKY, MYB and NAC-  
362 domain containing families are prominent among the regulatory genes induced by *crk10-*  
363 *A397T*, many of which have been associated with the modulation of stress responses  
364 (Supplemental Table S8). Therefore, biotic and abiotic stress-responsive pathways are  
365 constitutively activated in the *crk10-A397T* mutant, supporting our hypothesis that *crk10-*  
366 *A397T* is a gain-of-function allele of *CRK10*.

367 Furthermore, analysis of the lists of DEGs for each individual time point revealed  
368 that, specifically at 21 days, genes involved in the biosynthesis, signalling and homeostasis  
369 of the hormone abscisic acid (ABA) were also significantly up-regulated in the *crk10-A397T*  
370 mutant (Supplemental Table S9).

371

### 372 ***crk10-A397T* mutant hypocotyls contain increased levels of the stress hormones** 373 **salicylic acid (SA) and abscisic acid (ABA)**

374 In order to corroborate the transcriptomic data we quantified the levels of the stress  
375 hormones salicylic acid (SA), abscisic acid (ABA) and jasmonic acid (JA) from the

376 hypocotyls of 3-week-old WT and *crk10-A397T* plants (Supplemental Table S10). In  
377 agreement with the transcriptional induction of stress-responsive pathways, the levels of free  
378 SA and ABA were increased approximately 3 and 1.5 times, respectively, in the mutant  
379 hypocotyls. In contrast, JA levels were not significantly different to the WT.

380

381 **The *crk10-A397T* mutant displays enhanced resistant to infection by the vascular**  
382 **pathogen *Fusarium oxysporum* f. sp. *conglutinans* 699**

383 With defense responses constitutively up-regulated in the mutant, we next wanted to  
384 investigate whether this is reflected in an enhanced resistance to pathogens. Since *CRK10*  
385 expression is detected mainly in the vasculature, we chose the vascular pathogen *Fusarium*  
386 *oxysporum* f. sp. *conglutinans* 699, an isolate known to infect Arabidopsis for the assay  
387 (Masachis et al., 2016). *CRK10* OE-1 and *crk10-2* lines were also included in the experiment  
388 as overexpression and knockout of other CRKs often showed enhanced/decreased resistance  
389 phenotype to pathogens (Acharya et al., 2007, Yeh et al., 2015; Yadeta et al., 2017). The  
390 progression of the infection was observed (Figure 7A-D) and a time-mortality curve was  
391 recorded from 7 to 20 days post inoculation (Figure 7E). Our results showed that the  
392 susceptibility of WT and *crk10-2* plants to the pathogens was very similar, with both  
393 genotypes reaching over 65% of mortality at the end of the experiment. *CRK10* OE-1 and  
394 *crk10-A397T* plants exhibit a similarly low mortality rate until 10 days post inoculation,  
395 although *CRK10* OE-1 plants reach a final death toll of 47.5% in contrast to the lowest  
396 overall death count displayed by the *crk10-A397T* mutant of around 18%. Statistical analysis  
397 (Deviance test,  $\chi^2_3=19.68$ ,  $p < 0.001$ ) confirmed the differences in the probability of survival  
398 between genotypes, with the *crk10-A397T* mutant having the highest chance of survival of  
399 81.25%, followed by 52.5% for the *CRK10* OE-1 plants and just over 30% for both *crk10-2*  
400 and WT (Figure 7F). Fungal burden quantification by qPCR showed increased *F. oxysporum*  
401 biomass in WT and *crk10-2* plants compared to *CRK10* OE-1 and *crk10-A397T* mutant at 7  
402 days post inoculation, in agreement with the mortality trend results (Supplemental Figure  
403 S12). The experiment was performed twice with similar results. Therefore, our results  
404 strongly suggest that *crk10-A397T* mutant plants are more resistant to infection with *F.*  
405 *oxysporum*, reinforcing our hypothesis that the transcriptional responses induced by the  
406 *crk10-A397T* mutant allele are effective at reducing the spread of root-infecting vascular  
407 pathogens.

408

409

## DISCUSSION

410

411 Previous efforts to assign functions to specific CRKs mainly focused on the  
412 characterisation of T-DNA and overexpression lines. However, being a large multigene  
413 family, effects of knocking out one specific member are often masked by redundancy and, in  
414 the absence of known stimulants, overexpression lines are generally phenotypically  
415 indistinguishable from WT. Here we report the characterisation of the *crk10-A397T* mutant  
416 which harbours a gain-of-function allele of CRK10, to our knowledge the first such mutant  
417 obtained for this class of receptors in *Arabidopsis*.

418

### **The *crk10\_A397T* mutation lies in an important regulatory subdomain of the kinase domain of CRK10**

421 The point mutation responsible for the conversion of CRK10 into a gain-of-function  
422 allele (alanine 397 by threonine) lies in kinase subdomain III, right at the C-terminus of the  
423  $\alpha$ C-helix and at the start of the short  $\alpha$ C- $\beta$ 4 loop which links the  $\alpha$ C-helix to the  $\beta$  strand 4.  
424 The importance of this region for kinase regulation has been studied in numerous mammalian  
425 kinases with mutations residing in this area often leading to kinase de-regulation and disease,  
426 but equivalent studies in plant kinases are absent. The combined  $\alpha$ C-helix and  $\alpha$ C- $\beta$ 4 loop has  
427 been shown to be a critical allosteric docking site which plays a crucial part in kinase  
428 regulation (Yeung et al., 2020). As the 3D model of the CRK10 kinase domain suggests, the  
429 substituted amino acid lies on that surface of the helix, which faces away from the active site  
430 of the kinase and which is known to provide an interface for interactions with many  
431 regulatory domains and proteins. For human CDK2, for example, it was shown that residue  
432 Lys-56, equivalent to the position of Thr-397 in *crk10-A397T*, is involved in its interaction  
433 with cyclin necessary for the stabilisation of the active form of the kinase (Jeffrey et al.,  
434 1995), whereas in the case of the Ser/Thr-protein kinase B-Raf (BRaf), where dimerisation is  
435 thought to be an important part of the activation mechanism, the  $\alpha$ C-Helix/ $\alpha$ C- $\beta$ 4 loop  
436 provides the interface for dimer formation (Rajakulendran et al., 2009). This region can also  
437 function as a *cis*-regulatory site as shown for the human leucine-rich repeat kinase 2  
438 (LRRK2), where it provides a firm docking site for the C-terminal residues of the kinase  
439 which keeps it in an inactive conformation (Deniston et al., 2020, Taylor et al., 2020). As the

440  $\alpha$ C-helix/ $\alpha$ C- $\beta$ 4 loop is a feature common to all eukaryotic kinases, it seems reasonable to  
441 speculate that the amino acid substitution in *crk10-A397T* perturbs the interaction of CRK10  
442 with a regulatory partner. It is also noteworthy that the  $\alpha$ C helix and  $\alpha$ C- $\beta$ 4 loop is a highly  
443 conserved region within the family of CRKs and only three residues are found to occupy the  
444 position equivalent to Ala-397 of CRK10 among all the members: alanine, threonine or serine  
445 (Supplemental Figures S13 and S14). It now remains to be seen whether other members of  
446 the CRK-family are similarly affected by an analogous mutation in their  $\alpha$ C-helix/ $\alpha$ C- $\beta$ 4  
447 loops.

448

449 **Threonine 397 in the kinase domain of CRK10 is an auto-phosphorylation site *in***  
450 ***situ***

451 *In situ* phosphorylation analysis of the cytoplasmic kinase domains of WT and mutant  
452 CRK10 by LC-MS/MS determined that CRK10, being an RD kinase, shows the typical  
453 auto-phosphorylation pattern of conserved phosphorylation sites in the activation loop, on  
454 which the activity of this class of kinases is dependant (Nolen et al., 2004, Beenstock et al.,  
455 2016). Thr-507 and Ser-508 were identified as unambiguous phosphorylation sites, with Ser-  
456 508 likely to be functionally equivalent to Thr-450 of BAK1, which plays a key role in its  
457 activation by maintaining the active conformation of the activation loop (Yan et al., 2012).  
458 However, we also detected phosphorylation of tyrosine residues (Tyr-363 and Tyr-514), with  
459 Tyr-514 residing in the activation loop, which establishes CRK10 as a dual specificity kinase.  
460 Additional phosphorylated residues were detected in the juxtamembrane domain (Thr-340)  
461 and at the C-terminus (Thr-625, Ser-662 and Thr-664). Phosphorylation of residues in these  
462 non-catalytic regions have been shown to play an important role in the recognition and/or  
463 phosphorylation of downstream substrates, although these are unknown for CRKs (Wang et  
464 al., 2005; Oh et al., 2012; Zhou et al., 2020). The phosphorylation pattern of His-  
465 CRK100kd<sup>WT</sup> and His-CRK10kd<sup>A397T</sup> was identical, with the notable exception of the  
466 substituted Thr-397 functioning as an additional phosphorylation site in His-CRK10kd<sup>A397T</sup>.  
467 Based on the experimental evidence, it is currently not possible to distinguish whether Thr-  
468 397 *per se* or whether its phosphorylated form is the underlying cause for the phenotypic  
469 effects observed in the *crk10-A397T* mutant. The significance of the identified *in situ*  
470 phosphorylation sites for CRK10 activity *in vivo* also remains to be determined.

471

472           **The dwarf phenotype of the *crk10-A397T* mutant is linked to the collapse of**  
473 **xylem vessels in roots and hypocotyls**

474           Phenotypically, the *crk10-A397T* mutant is a dwarf, which we showed to be the  
475 consequence of collapsed xylem elements in the roots and hypocotyl. Collapsed xylem  
476 vessels are thought to occur due to alterations in the cell wall composition, leading to cell  
477 wall weakening and a consequent inability to withstand the negative pressure generated by  
478 transpiration, as reported in the *eskimo* and *irx* mutants, for example (Turner & Somerville,  
479 1997; Lefebvre et al., 2011). Although secondary cell wall defects are generally readily  
480 observed when analysed by TEM, we could not detect any obvious differences in the  
481 vessel cell wall ultrastructure in cross sections of 3-week-old hypocotyls of the *crk10-A397T*  
482 mutant and WT. Considering the severity of the vessel collapse in the mutant this was  
483 unexpected and future analysis of the composition of the cell wall will be necessary in order  
484 to determine the biochemical defects. Intriguingly, although *CRK10* is expressed in vascular-  
485 associated tissues in both stem and hypocotyl as shown by reporter lines and qPCR analysis,  
486 xylem elements in the stem seem to develop normally in the mutant. Why xylem elements are  
487 defective in one organ but not the other can, therefore, not simply be explained by a restricted  
488 expression pattern of *CRK10* but, considering that RLKs usually reside in large complexes at  
489 the plasma membrane, might be due to tissue-specific composition of the “receptorsomes”.  
490 However, grafting experiment strongly suggest that it is the defective vasculature in the  
491 belowground organs causing the dwarf phenotype, as WT scions grafted onto *crk10-A397T*  
492 rootstocks become similarly stunted whereas *crk10-A397T* scions grafted on WT rootstocks  
493 develop normally.

494

495           **Stress responses are constitutively activated in the hypocotyl of *crk10-A397T***

496           Collapsed vessel elements are thought to impede proper water transport which is  
497 likely to be perceived as drought stress leading to an increase of ABA. This could explain the  
498 elevated levels of ABA which we detected in the hypocotyl of *crk10-A397T* and the up-  
499 regulation of genes involved in ABA synthesis, perception and response (Supplemental Table  
500 S9). A similar increase in ABA levels has been observed in other cell wall mutants such as  
501 *esk1* and *irx1-6* whereas *irx3*, *irx5* and *irx9* contained numerous constitutively up-regulated  
502 ABA-responsive genes (Chen et al., 2005; Hernández-Blanco et al., 2007; Lefebvre et al.,  
503 2011; Faria-Blanc et al., 2018; Xu et al., 2020). The stunting of these mutants has been

504 suggested to be the consequence of the response to drought signalling hormones resulting in  
505 the suppression of growth, which could also explain the dwarfism of *crk10-A397T*. It will be  
506 interesting to investigate whether dwarfing of *crk10-A397T* can be alleviated by an ABA  
507 insensitive mutant such as *abil* (Koornneef et al., 1984).

508         The severe collapse of the xylem elements in the roots and hypocotyl of *crk10-A397T*  
509 is most likely due to alterations of the composition of the cell walls and it is increasingly  
510 being reported that modification of cell wall composition by genetic or chemical means leads  
511 to the constitutive activation of defense pathways and an altered resistance to pathogens. The  
512 primary cell wall mutant *ixr1/cev1*, for example, with reduced crystalline cellulose content  
513 due to the defective cellulose synthase CESA3, displays constitutive activation of jasmonic  
514 acid and ethylene signalling (Ellis et al., 2001; Ellis et al., 2002). Transcriptomic data  
515 obtained for the secondary cell wall mutants *irx1-6*, *irx5-5* and *irx9* showed that defense-  
516 related genes are constitutively expressed in these mutants (Hernández-Blanco et al., 2007;  
517 Faria-Blanc et al., 2018). In line with these reports, our data showed that the signature of the  
518 core set of DEGs of *crk10-A397T* was most similar to the transcriptome of plants responding  
519 to biotic and abiotic stress. Canonical SA-dependent marker genes (PR1, PR2 and PR5) and  
520 genes involved in the synthesis of the tryptophan-derived antimicrobial compounds  
521 (camalexin, glucosinolates) are significantly up-regulated in the mutant, as are numerous  
522 transcription factors usually associated with coordinating stress responses (Supplemental  
523 Tables S7 and S8). Concomitant with gene induction, SA levels in the *crk10-A397T* mutant  
524 hypocotyls are increased, whereas changes in JA levels were not significant. Induction of  
525 defense pathways due to cell wall impairment manifests itself frequently in alteration of  
526 disease resistance to a wide range of pathogens (Houston et al., 2016; Bacete et al., 2018).  
527 Molina et al. (2021), for example, showed that from a panel of 34 cell wall mutants affecting  
528 a wide range of different cell wall compounds, 29 had an altered, mainly enhanced, resistance  
529 response to pathogens comprising different parasitic lifestyles. In order to assess disease  
530 resistance of *crk10-A397T* we chose the root-infecting, hemi-biotrophic vascular wilt  
531 pathogen *F. oxysporum* to perform a pathogen assay, bearing in mind the vasculature  
532 associated expression of *CRK10*. In agreement with the studies linking cell wall modification  
533 to altered disease resistance, we found that the *crk10-A397T* mutant was significantly more  
534 resistant to the pathogen, part of which could be due to the fact that collapsed xylem vessels  
535 act as physical barriers slowing pathogen progression in the roots.

536

## 537 **Conclusion**

538 Taken together, the experimental evidence provided in this report suggests that *crk10-*  
539 *A397T* is a mutant which contains a gain-of function allele of the cysteine rich receptor-like  
540 kinase CRK10. The transcriptome of the mutant carries the typical signature of a plant  
541 responding to stress, although at this stage it is not possible to differentiate whether the stress  
542 response is the direct consequence of spontaneous signalling occurring because of the  
543 mutated CRK10 receptor or whether it is the response to the perception of the defective  
544 xylem vessel cell walls. The mutation lies in the  $\alpha$ C-Helix/ $\alpha$ C- $\beta$ 4 loop which is emerging as a  
545 key structural element in the regulation of kinase function and regulation and a hot-spot for  
546 post-translational modifications (Yeung et al., 2020). It is noteworthy that the only other  
547 semi-dominant mutant reported for a CRK in rice, *als1*, which develops spontaneous lesions  
548 on leaf blades and sheaths also localises to this loop (Du et al., 2019). Future work will now  
549 need to address the consequence of the *A397T* mutation for kinase activity. The dwarf and  
550 collapsed xylem phenotype of the *crk10-A397T* mutant could, for example, be caused by  
551 CRK10 having been converted into a constitutively active kinase and thereby reflect the  
552 function of wild type CRK10. However, another scenario which needs to be taken into  
553 consideration is that CRK10 *A397T* has assumed a novel function and interferes with an  
554 endogenous pathway distinct from the normal mode of action of wild type CRK10.

555

## 556 **FIGURE LEGENDS**

557

558 **Figure 1** CRK10 and CRK10-A397 are active kinases and the A397T substitution  
559 introduces an additional auto-phosphorylation site in the kinase domain of the protein. A,  
560 Amino acid sequence of the cytoplasmic kinase domain of CRK10 used for in situ  
561 phosphorylation studies (CRK10 amino acid residue numbering shown on the left).  
562 Subdomains I-XI are indicated by roman numerals. Ala/Thr 397 site is highlighted in red, and  
563 the RD motif is underlined and highlighted in bold. The conserved glycine-rich loop,  
564 catalytic loop and activation segment motifs are also shown. B, Structure of the CRK10  
565 kinase domain generated by homology modelling to the active kinase domain of BRI1. A  
566 molecule of an ATP analogue, coloured blue, occupies the active site. The  $\alpha$ C-helix is  
567 coloured red, and the atoms in the side chain of the mutated threonine residue are depicted as

568 red spheres. C, Recombinant His-CRK10kd<sup>WT</sup> and His-CRK10kd<sup>A397T</sup> extracts and their  
569 respective dead kinase controls (His-CRK10kd<sup>WT</sup>-D473N and His-CRK10kd<sup>A397T</sup>-D473N)  
570 resolved by SDS-PAGE; detection by Western blot with HRP-conjugated anti-His antibody is  
571 shown. D, SDS-PAGE and Western blot following treatment of purified His-tagged proteins  
572 with  $\lambda$ -phosphatase (PPase); control: untreated protein. E, In situ auto-phosphorylation sites  
573 in His-CRK10kd<sup>WT</sup> and His-CRK10kd<sup>A397T</sup> identified by LC-MS/MS analysis of the  
574 recombinant protein kinase domain. Threonine 397 is highlighted in red. His: 6x His-tag; JM:  
575 juxta-membrane domain; KD: kinase domain; C-term tail: C-terminal tail. (f) MS/MS  
576 spectrum of the doubly charged (m/z 758.4) tryptic phosphopeptide NEVVLVTKLQHR in  
577 which the threonine residue is phosphorylated. Neutral losses of phosphoric acid from both  
578 the precursor ion and the C-terminal y ions are observed.

579

580 **Figure 2** *crk10-A397T* mutant is a dwarf. A-F, Rosette morphology of WT (A, B, C)  
581 and *crk10-A397T* (D, E, F) plants at 2 (A, D), 3 (B, E) and 4 (C, F) weeks after sowing. Bar =  
582 1 cm. G, Leaf series of 4-week-old WT (top) and *crk10-A397T* (bottom) plants. Bar = 1 cm.  
583 H, Main inflorescence stem of 5-week-old WT (left) and *crk10-A397T* (right) plants. Bar = 1  
584 cm. I, 10-week-old WT (left) and *crk10-A397T* (right) plants. Bar = 2 cm. J, Siliques of WT  
585 (left) and *crk10-A397T* (right) plants. Bar = 1 cm. K, Seeds of WT (left) and *crk10-A397T*  
586 (right) plants. Bar = 500  $\mu$ m.

587

588 **Figure 3** Xylem vessels collapse in the root and hypocotyl of *crk10-A397T* plants, but  
589 not in the stem. A-F, Transverse cross sections of the base of stem (A, B), hypocotyl (C, D)  
590 and roots (E, F) of 5-week-old WT (A, C, E) and *crk10-A397T* (B, D, F) plants. Stain:  
591 potassium permanganate. Bars = (A, B, C, E, F) 100  $\mu$ m; (D) 50  $\mu$ m. G-H, Detail of xylem  
592 vessels in hypocotyls of 4-week-old WT (G) and *crk10-A397T* (H) mutant plants. Stain:  
593 potassium permanganate. Insert in top left corner of image shows original micrographs. Bars  
594 = (insert G) 50  $\mu$ m; (insert H) 25  $\mu$ m. I-J, Detection of auto-fluorescence of lignin on resin-  
595 embedded cross sections of 4-week-old hypocotyls of WT (I) and *crk10-A397T* (J) plants.  
596 Bars = 10  $\mu$ m.

597

598 **Figure 4** CRK10 is a plasma membrane-localised protein expressed in association  
599 with the vasculature in the hypocotyl. A-B, Histochemical staining of reporter lines

600 expressing the *CRK10*<sub>Pro</sub>:*GUS* construct showed expression of the reporter gene in the  
601 vasculature of stem and hypocotyls, as shown by free-hand cross section of 8-week-old  
602 inflorescence stem (A) and cross section of 2-week-old hypocotyl embedded in resin (B).  
603 Bars = (A) 50  $\mu\text{m}$ ; (B) 25  $\mu\text{m}$ . C, Detail of cross section in B shows presence of  
604 histochemical staining in xylem parenchyma cells (asterisks) and differentiating xylem  
605 vessels (arrows) in the hypocotyl. C-D, Hypocotyl of 4-day-old seedling of transgenic  
606 *Arabidopsis* plant expressing 35S:*CRK10-mCherry* before (C) and after (D) plasmolysis.  
607 Bars = 20  $\mu\text{m}$ .

608

609 **Figure 5** The root-hypocotyl system is responsible for the dwarf phenotype of *crk10-*  
610 *A397T* mutant plants. Images of non-grafted plants (A), self-graft controls (B) and graft  
611 combinations (C) of WT and *crk10-A397T* mutant. Plants were imaged 3 weeks after  
612 micrografting was performed. The phenotype observed for the reciprocal grafting  
613 combinations were consistently observed in two independent repetitions of the experiment.  
614 An average number of 10 grafts per combination was recovered each time. Annotation: scion  
615 / rootstock.

616

617 **Figure 6** Transcriptional reprogramming in the *crk10-A397T* mutant shows activation  
618 of defense responses to biotic and abiotic stresses. A, Venn diagram displaying the number of  
619 differentially expressed genes (DEGs) in the *crk10-A397T* hypocotyls compared to the WT at  
620 each developmental time point. B, Top 15 enriched GO terms (Biological Process) for the up-  
621 regulated core DEGs in the *crk10-A397T* mutant plotted against their respective  $-\log_{10}$  FDR.  
622 C, Top 15 perturbations showing highest overall similarity to *crk10-A397T* mutant expression  
623 signature (analysis performed using the GENEVESTIGATOR® SIGNATURE tool;  $\log_2$  fold  
624 change values of time point 21 days was used as input for 274 core genes).

625

626 **Figure 7** *crk10-A397T* mutant plants are more resistant to infection with *Fusarium*  
627 *oxysporum* f. sp. *conglutinans* 699. A-D, Representative images of WT (A), *crk10-2* (B),  
628 *CRK10* OE-1 (C) and *crk10-A397T* mutant (D) plants at 11 days post inoculation with *F.*  
629 *oxysporum*. E, Mortality curve of WT, *crk10-A397T*, *CRK10* OE-1 and *crk10-2* plants from  
630 day 7 to 20 post inoculation with *F. oxysporum*. Mortality is shown in percentage. The  
631 experiment was repeated twice with similar results. F, Probability of survival of each

632 genotype following inoculation with the pathogen *F. oxysporum*. Associated 95% confidence  
633 intervals are shown. Deviance test,  $\chi^2_3=19.68$ ,  $p < 0.001$ .

634

## 635 MATERIALS AND METHODS

636

### 637 Plant Materials and Growth Conditions

638 *Arabidopsis thaliana* ecotype Col-0 plants were grown in Grobanks cabinets (CLF  
639 2006, Plant Climatics, Germany) in Levington F2 + Sand compost in long day conditions  
640 (16h/8h), 23/18 °C day/night temperature, 200  $\mu\text{mol m}^{-2} \text{sec}^{-1}$  of light intensity. For *in vitro*  
641 experiments, surface sterilized seeds were placed on ½ MS plates (Murashige & Skoog,  
642 Duchefa Biochemie).

643

### 644 RNA-Seq

645 Total RNA was extracted from hypocotyls of *Arabidopsis* plants using the RNeasy  
646 Mini Kit (QIAGEN), and samples were subsequently treated with DNase Turbo DNA-free kit  
647 (Thermo Fisher Scientific). Each biological replicate consisted of a pool of 50-60 hypocotyls,  
648 and four biological replicates were isolated per genotype per time point. RNA quality was  
649 assessed on a 2100 Bioanalyzer (Agilent Technologies). Library preparation and paired-end  
650 sequencing, Illumina HiSeq 125 PE sequencing was performed by Exeter Sequencing Service  
651 (University of Exeter, UK). The Rothamsted instance of the Galaxy (<https://usegalaxy.org/>)  
652 bioinformatics web pipeline was used to perform quality control (MultiQC;  
653 <https://multiqc.info/>), trimming (Trimmomatic; Bolger et al., 2014) and mapping to the  
654 reference genome (HiSAT2; Kim et al., 2015). The table of counts was acquired using the  
655 featureCounts functions in the Subread (Liao et al., 2019;  
656 <https://bioconductor.org/packages/release/bioc/html/Rsubread.html>) on the R Bioconductor  
657 platform (<https://bioconductor.org/>). Genes with less than 3 samples with counts  $\geq 5$  were  
658 discarded. Differentially expressed genes were identified (using the default Wald test) in the  
659 R (v3.6.1) Bioconductor package DESeq2 (Love et al., 2014;  
660 <https://bioconductor.org/packages/release/bioc/html/DESeq2.html>). Gene Ontology (GO)  
661 enrichment analysis (Single Enrichment Tool, AgriGO v2.0; Tian et al., 2017) and similarity  
662 comparison with deposited micro-array datasets (Signature tool, GENEVESTIGATOR®,  
663 Hruz et al., 2008) were performed for the set of 274 core differentially expressed genes.

664

### 665 **Quantitative PCR**

666 RNA was isolated using TRI Reagent® (Merck) and treated with DNase I,  
667 Amplification Grade (Thermo Fisher Scientific) prior to cDNA synthesis with SuperScript™  
668 III Reverse Transcriptase (Thermo Fisher Scientific). All qPCR reactions were performed in  
669 a LightCycler® 96 Real-Time PCR System (Roche Diagnostics) using the FastStart Essential  
670 DNA Green Master (Roche Diagnostics). *ACTIN2* (AT3G18780) and *UBC21* (AT5G25760)  
671 were used as internal controls (Supplemental Table S11), and the  $2^{-\Delta\Delta Ct}$  method (Livak &  
672 Schmittgen, 2001) was used to calculate relative expression.

673

674

675

### 676 **Quantification of plant hormones**

677 Hypocotyl samples (75 – 100 mg fresh weight) isolated from 3-week-old plants were  
678 used for the quantification of hormones as described in Camut et al., 2019. A 2.6 µm  
679 Accucore RP-MS column (100 mm length x 2.1 mm i.d.; ThermoFisher Scientific) and a Q-  
680 Exactive mass spectrometer (Orbitrap detector; ThermoFisher Scientific) were used. The  
681 concentrations of hormones in the extracts were determined using embedded calibration  
682 curves and the Xcalibur 4.0 and TraceFinder 4.1 SP1 programs. Three biological replicates  
683 per genotype were analysed.

684

### 685 **Cloning of genetic constructs**

686 The list of primers used in this study can be found in Supplemental Table S11. To  
687 generate the construct for the complementation of the *crk10-A397T* mutant and  
688 overexpression of *CRK10* in the WT plants, the cDNA sequence of *CRK10* was amplified  
689 from the cDNA clone U60398 with *SalI* and *SacI* restriction sites and cloned into pJD330  
690 downstream of the 35S promoter. The construct 35S:*CRK10*-NOS was then amplified with  
691 *AscI* restriction sites and cloned into the RS 3GSeedDSRed MCS vector. To obtain the  
692 *CRK10<sub>Pro</sub>:crk10-A397T*-NOS construct, the 1 kb genomic sequence upstream of *CRK10*  
693 (*CRK10<sub>Pro</sub>*) was amplified from Arabidopsis Col-0 genomic DNA with *SphI* and *SalI*  
694 restriction sites, and was cloned in pJD330 upstream of the *CRK10* cDNA sequence. The  
695 G>A mutation harboured by the *crk10-A397T* mutant was introduced by *in vitro* mutagenesis.

696 The *CRK10*<sub>Pro</sub> sequence was amplified with *SphI* and *NcoI* restriction sites, and the fragment  
697 was ligated upstream of the  $\beta$ -glucuronidase (*GUS*) gene in pJD330. The *CRK10*<sub>Pro</sub>:*GUS*-  
698 NOS construct was amplified with *AscI* restriction sites and cloned into the RS  
699 3GSeedDSRed MCS vector. To obtain a translational fusion of CRK10 with the fluorescent  
700 protein mCherry, the stop codon of *CRK10* was removed and a *SacI* restriction site was  
701 introduced by *in vitro* mutagenesis between *CRK10* and the NOS terminator sequence in  
702 pJD330. The coding sequence of *mCherry* was cloned with *SacI* restriction sites on both ends  
703 and ligated in frame with *CRK10*. The construct *CRK10-mCherry*-NOS was then amplified  
704 with *SalI* and *NotI* restriction sites and cloned into pENTR1A Dual Selection Vector  
705 (Invitrogen). Following LR reaction (Gateway) with the binary vector pB2GW7 (Invitrogen),  
706 the construct 35S:*CRK10-mCherry*-NOS was obtained. Finally, to generate the constructs for  
707 recombinant protein in *E. coli*, the coding sequence of the kinase domain of *CRK10* was  
708 amplified with *SalI* and *NotI* restriction sites and cloned into pENTR1A Dual Selection  
709 Vector (Invitrogen) prior to recombination with pDEST17 (Invitrogen), where it was cloned  
710 in frame with an N-terminal 6x His-tag. *In vitro* mutagenesis was used to generate the gain-  
711 of-function mutation of CRK10 (A397T) as well as the dead kinase variant by mutation of  
712 the invariant aspartic acid in the active site to an asparagine (D473N). All constructs used for  
713 the generation of transgenic plants were introduced in *A. tumefaciens* cells strain GV3101  
714 using the freeze and thaw protocol (An et al., 1988), and the floral dip method (Clough and  
715 Bent, 1998) was used to transform *Arabidopsis* plants.

716

### 717 **Transient expression of fluorescent fusion in *N. benthamiana***

718 Protocol was adapted from Sparkes et al., 2006. Transient expression of the fusion  
719 protein was observed 72 hours post-infiltration.

720

### 721 **Microscopy**

722 For the preparation of thin sections for light microscopy, plant tissue samples were  
723 fixed in 4% paraformaldehyde / 2.5% glutaraldehyde (0.05 M phosphate buffer pH 7.2),  
724 dehydrated in graded ethanol series (10 – 100%) and infiltrated with LRWhite resin (Agar  
725 Scientific). Sections were prepared using a Reichert Ultramicrotome (section thickness: 1-2  
726  $\mu$ m) and stained with 0.5% potassium permanganate. Thin sections were observed with a  
727 Zeiss Axiophot equipped with a Q-Imaging Retiga EXi CCD mono digital camera with RGB

728 filter wheel (QImaging, Canada) coupled with the Metamorph software (Molecular Devices,  
729 USA). Non-stained resin embedded thin sections were also used for the detection of the auto-  
730 fluorescence of lignin using the confocal microscope (excitation: 405 nm; emission: 451-480  
731 nm and 560-612 nm). For the detection of mCherry fluorescence from *N. benthamiana* leaves  
732 and hypocotyls of Arabidopsis, a small piece of fresh tissue sample was mounted on a glass  
733 slide with glass cover slip and water, and the fluorescence was detected using the confocal  
734 microscope (excitation: 561 nm laser; emission: 578 - 639 nm). Plasmolysis was performed  
735 using a 0.8M mannitol solution for 40 minutes and images acquired prior to and after  
736 treatment. Fluorescent signals were detected from thin sections and whole plant samples  
737 using a Zeiss 780 LSM confocal microscope. For the preparation of samples for transmission  
738 electron microscopy (TEM), plant material was fixed by high-pressure freezing in 0.1 M  
739 sucrose using a Leica HPM100, followed by freeze substitution with 100% ethanol (Leica  
740 EM Auto Freeze substitution) and infiltration with LRWhite resin (Agar Scientific). Ultra-  
741 thin sections prepared with a Leica EM UCT Ultramicrotome (section thickness: 90 nm) were  
742 collected on pioloform/carbon-coated nickel grids (Agar Scientific) and stained with 2.5%  
743 uranyl acetate and Reynolds lead citrate (Reynolds, 1963). Ultrathin sections were imaged  
744 using a JEOL-2100Plus Transmission Electron Microscope (JEOL, Japan) equipped with a  
745 Gatan OneView IS Camera (Gatan, USA).

746

#### 747 **Micrografting of Arabidopsis seedlings**

748 Grafting protocol was performed as previously described (Turnbull et al., 2002).  
749 Successful grafts were transferred to soil 7-10 days post-grafting.

750

#### 751 **GUS staining**

752 Plant tissue was incubated overnight in X-Gluc (Melford) solution at 37 °C.  
753 Chlorophyll was removed with 80% ethanol prior to imaging using a Leica M205 FA  
754 Stereomicroscope (Leica Microsystems).

755

#### 756 **Recombinant protein expression, purification and analysis**

757 BL21 AI One-Shot E. coli cells (Invitrogen) were used for the expression of  
758 recombinant 6x His-tag CRK10 kinase domain variants. Singles colonies were inoculated in  
759 liquid media supplemented with antibiotics and 0.1% glucose and grown overnight at 37 °C

760 shaking at 225 rpm. A 250  $\mu$ L aliquot of the overnight culture was used to inoculate 50 mL of  
761 fresh selective media, and cells were grown until  $OD_{600} = 0.4-0.5$  was obtained. L-arabinose  
762 was added to the cultures to a final concentration of 0.2% to induce expression of the  
763 recombinant protein, and cultures were grown for an additional 3 hours. Cells were harvested  
764 by centrifugation (5,000 g x g for 10 minutes), resuspended in equilibration buffer (50 mM  
765 sodium phosphate pH 8.0, 0.3 M sodium chloride) and lysed by sonication. The cell lysate  
766 was centrifuged for 30 minutes at 5,000 x g and the supernatant was recovered and mixed  
767 with HIS-Select Nickel Affinity Gel (Sigma Aldrich) for protein purification (manufacturer's  
768 instructions were followed). The concentration of the purified protein extracts was measured  
769 using the Bradford method (Protein Assay Dye Reagent, Bio-Rad). Purified His-tagged  
770 proteins were resolved by SDS-PAGE (NuPAGE 4-12% Bis-Tris Protein Gels, Invitrogen)  
771 and gels were stained with Quick Coomassie Stain (Generon). Alternatively, proteins were  
772 transferred to a PVDF membrane (iBlot Transfer Stack, PVDF, Invitrogen) for Western  
773 blotting. The membrane was blocked with 5% powder milk in PBS-T, and incubated with  
774 His-probe (H-3) HRP monoclonal antibody (Santa Cruz Biotechnology) for 1 hour. The  
775 membrane was washed and incubated with Amersham ECL Western Blotting Detection  
776 Reagent (GE Healthcare) and developed in the dark. Protein extracts were also treated with  
777 Lambda Protein Phosphatase (Lambda PP, New England BioLabs) according to the  
778 manufacturer's protocol. Briefly, 5  $\mu$ g of purified protein were incubated with Lambda PP for  
779 1h30min at 30 °C. Phosphatase-treated samples were then resolved on SDS-PAGE and  
780 detected by Western blotting.

781

### 782 **Liquid chromatography – Mass Spectrometry/Mass Spectrometry (LC-MS/MS)** 783 **and MASCOT database search**

784 Gel bands were transferred into a 96-well PCR plate. Peptide bands were cut into  
785 1mm<sup>2</sup> pieces, destained, reduced (DTT) and alkylated (iodoacetamide) and subjected to  
786 enzymatic digestion with sequencing grade trypsin (Promega, Madison, WI, USA) overnight  
787 at 37°C. After digestion, the supernatant was pipetted into a sample vial and loaded onto an  
788 autosampler for automated LC-MS/MS analysis. All LC-MS/MS experiments were  
789 performed using a Dionex Ultimate 3000 RSLC nanoUPLC (Thermo Fisher Scientific Inc,  
790 Waltham, MA, USA) system and a QExactive Orbitrap mass spectrometer (Thermo Fisher  
791 Scientific Inc, Waltham, MA, USA). Separation of peptides was performed by reverse-phase

792 chromatography at a flow rate of 300 nL/min and a Thermo Scientific reverse-phase nano  
793 Easy-spray column (Thermo Scientific PepMap C18, 2  $\mu\text{m}$  particle size, 100A pore size, 75  
794  $\mu\text{m}$  i.d. x 50cm length). Peptides were loaded onto a pre-column (Thermo Scientific PepMap  
795 100 C18, 5  $\mu\text{m}$  particle size, 100A pore size, 300  $\mu\text{m}$  i.d. x 5mm length) from the Ultimate  
796 3000 autosampler with 0.1% formic acid for 3 minutes at a flow rate of 10  $\mu\text{L}/\text{min}$ . After this  
797 period, the column valve was switched to allow elution of peptides from the pre-column onto  
798 the analytical column. Solvent A was water + 0.1% formic acid and solvent B was 80%  
799 acetonitrile, 20% water + 0.1% formic acid. The linear gradient employed was 2-40% B in 30  
800 minutes. Further wash and equilibration steps gave a total run time of 60 minutes. The LC  
801 eluant was sprayed into the mass spectrometer by means of an Easy-Spray source (Thermo  
802 Fisher Scientific Inc.). All  $m/z$  values of eluting ions were measured in an Orbitrap mass  
803 analyzer, set at a resolution of 70000 and was scanned between  $m/z$  380-1500. Data  
804 dependent scans (Top 20) were employed to automatically isolate and generate fragment ions  
805 by higher energy collisional dissociation (HCD, NCE:25%) in the HCD collision cell and  
806 measurement of the resulting fragment ions was performed in the Orbitrap analyser, set at a  
807 resolution of 17500. Singly charged ions and ions with unassigned charge states were  
808 excluded from being selected for MS/MS and a dynamic exclusion window of 20 seconds  
809 was employed.

810

### 811 **Protein modelling**

812 A structural model of the kinase domain of CRK10 was generated by homology  
813 modelling using PyMOD 3.0 with default parameters (Janson et al., 2017). The kinase  
814 domain of BRI1 (PDB code 5LPV) (Bojar et al., 2014) was used as template retaining the  
815 ATP analogue (phosphoaminophosphonic acid-adenylate ester) but no other heteroatoms.

816

### 817 **Plant infection assay**

818 Root infection assay was modified from Masachis et al., 2016. Arabidopsis seedlings  
819 (12-days-old) grown *in vitro* were inoculated by immersing their roots for 20 minutes in a  
820 suspension of  $1 \times 10^6$  microconidia  $\text{ml}^{-1}$  of *F. oxysporum* f. sp. *conglutinans* 699. Seedlings  
821 were transferred to Levington F2 + Sand compost with vermiculite (3:1) and incubated in  
822 growth chamber under long day conditions (16/8h), 28/25  $^{\circ}\text{C}$  day/night temperature. Eighty  
823 plants per genotype were planted in a randomised blocked tray design, and mortality was

824 assessed daily between 7 and 20 days post-inoculation. For determination of fungal burden,  
825 three independent replications of the experiment were performed. Seedlings were inoculated  
826 as described above and collected at 2 and 7 days post-inoculation. Each repetition of the  
827 experiment included one pool of eight seedlings per genotype which were processed as one  
828 biological replicate. Total DNA extraction was performed according to Yu et al., 2019 and  
829 the relative amount of fungal DNA was quantified by qPCR using the *F. oxysporum ACTINI*  
830 normalized to the Arabidopsis *ACTIN2* gene. Results were expressed relative to WT at 2 days  
831 post inoculation.

832

### 833 **Statistical analysis**

834 Statistical tests were performed using the Genstat software (Genstat for Windows 21st  
835 Edition; VSN International, Hemel Hempstead, UK). Student's t-test were used to assess  
836 statistical differences between two variants. To assess whether the pattern of segregation of  
837 the dwarf phenotype followed the expected 1:2:1 ratio, the  $\chi^2 = \sum_{i=1}^r \frac{(O_i - E_i)^2}{E_i}$  chi-square  
838 statistic was used, where  $O_i$  is the observed count for group  $i$  and  $E_i$  is the expected count for  
839 group  $i$ . Under the null hypothesis of 1:2:1 segregation this test statistic should follow a chi-  
840 square distribution with 2 degrees of freedom. The probability of survival of each genotype in  
841 the bioassay with *F. oxysporum* was assessed with a generalized linear model (Bernoulli  
842 distribution; logit link function fitted to the final mortality outcome of each plant); statistical  
843 significance of the genotypic effect was tested after removing variation associated with plant  
844 position within rows of different trays and quantified through a Chi-squared statistic of the  
845 difference in deviance. Statistical significance of the differences in fungal burden between  
846 genotypes were tested by ANOVA (expression levels were log-transformed to meet the  
847 ANOVA requirements, and each individual experiment was considered as a block).

848

### 849 **Accession numbers**

850 Gene sequence data for this article can be found in The Arabidopsis Information  
851 Resource (TAIR) under the accession number AT4G23180 (*CRK10*). The *CRK10* cDNA  
852 clone (U60398) was obtained from the Arabidopsis Biological Resource Center (ABRC). The  
853 T-DNA lines SAIL\_427\_E09 and SALK\_116653 were obtained from the Nottingham  
854 Arabidopsis Stock Centre (NASC; plants were genotyped according to instructions provided  
855 in <http://signal.salk.edu>). The mass spectrometry proteomics data have been deposited to the

856 ProteomeXchange Consortium via the PRIDE (Perez-Riverol et al., 2019) partner repository  
857 with the dataset identifier PXD023831.

858

## 859 ACKNOWLEDGMENTS

860 We thank Professor Colin Turnbull (Imperial College London) for help with the  
861 micrografting technique; Hannah Walpole, Kirstie Halsey and Dr Eudri Venter (Bioimaging  
862 Department, Rothamsted Research) for assistance with light, confocal and transmission  
863 electron microscopy; Dr Jason Rudd (Department of Biointeractions and Crop Protection,  
864 Rothamsted Research) for invaluable discussions regarding the analysis of the kinase domain  
865 of CRK10; Dr Kim Hammond-Kosack (Department of Biointeractions and Crop Protection,  
866 Rothamsted Research) for insightful discussions regarding CRK10's role in plant-pathogen  
867 interactions; Kirsty Hassall (Department of Computational and Analytical Sciences,  
868 Rothamsted Research) for support with experimental design and statistical analyses; and  
869 Professor Antonio di Pietro for providing the fungal isolate used in this study. We thank the  
870 University of Exeter for the Exeter International Excellence Scholarship which supported MP  
871 while this work was developed. This work was supported by UK Biotechnology and  
872 Biological Sciences Research Council grants BBS/E/C/000I0420 and BB/P016855/1. This  
873 research was done under the regulation described in the DEFRA license number  
874 101948/198285/6.

875

## 876 REFERENCES

877 **Acharya BR, Raina S, Maqbool SB, Jagadeeswaran G, Mosher SL, Appel HM, Schultz**  
878 **JC, Klessig DF, Raina R** (2007) Overexpression of *CRK13*, an Arabidopsis cysteine-rich  
879 receptor-like kinase, results in enhanced resistance to *Pseudomonas syringae*. *Plant Journal*  
880 **50**: 488-499

881 **Ahuja I, Kissen R, Bones AM** (2012) Phytoalexins in defense against pathogens. *Trends in*  
882 *Plant Sciences* **17**: 73-90

883 **An G, Ebert PR, Mitra A, Ha SB** (1988) Binary vectors. In: Gelvin SB, Schilperoot RA  
884 eds. *Plant Molecular Biology Manual*. Kluwer, Dordrecht, Netherlands, A3:1-19

885 **Bacete L, Melida H, Miedes E, Molina A** (2018) Plant cell wall-mediated immunity: cell  
886 wall changes trigger disease resistance responses. *Plant Journal* **93**: 614-636

- 887 **Beenstock J, Mooshayef N, Engelberg D** (2016) How Do Protein Kinases Take a Selfie  
888 (Autophosphorylate)? Trends in Biochemical Sciences **41**: 938-953
- 889 **Bojar D, Martinez J, Santiago J, Rybin V, Bayliss R, Hothorn M** (2014) Crystal  
890 structures of the phosphorylated BRI1 kinase domain and implications for brassinosteroid  
891 signal initiation. Plant Journal **78**: 31-43
- 892 **Bolger AM, Lohse M, Usadel B** (2014) Trimmomatic: a flexible trimmer for Illumina  
893 sequence data. Bioinformatics **30**: 2114-2120
- 894 **Bourdais G et al. CRK Consortium** (2015) Large-Scale Phenomics Identifies Primary and  
895 Fine-Tuning Roles for CRKs in Responses Related to Oxidative Stress. PLoS Genetics **11**:  
896 e1005373
- 897 **Camut L, Regnault T, Sirlin-Josserand M, Sakvarelidze-Achard L, Carrera E, Zumsteg  
898 J, Heintz D, Leonhardt N, Lange MJP, Lange T et al.** (2019) Root-derived GA12  
899 contributes to temperature-induced shoot growth in Arabidopsis. Nature Plants **5**:1216-1221
- 900 **Chen Z.** (2001) A Superfamily of Proteins with Novel Cysteine-Rich Repeats. Plant  
901 Physiology **126**: 473-476
- 902 **Chen Z, Hong X, Zhang H, Wang Y, Li X, Zhu JK, Gong Z** (2005) Disruption of the  
903 cellulose synthase gene, *AtCesA8/IRX1*, enhances drought and osmotic stress tolerance in  
904 Arabidopsis. Plant Journal **43**: 273-283
- 905 **Chinchilla D, Bauer Z, Regenass M, Boller T, Felix G** (2006) The Arabidopsis receptor  
906 kinase FLS2 binds flg22 and determines the specificity of flagellin perception. Plant Cell **18**:  
907 465-476
- 908 **Clough S, Bent A** (1998) Floral dip: A simplified method for Agrobacterium-mediated  
909 transformation of Arabidopsis thaliana. Plant Journal **16**: 735-743
- 910 **Czernic P, Visser B, Sun W, Savouré A, Deslandes L, Marco Y, Van Montagu M,  
911 Verbruggen N** (1999) Characterization of an *Arabidopsis thaliana* receptor-like protein  
912 kinase gene activated by oxidative stress and pathogen attack. The Plant Journal **18**: 321-327
- 913 **De Smet I, Voß U, Jürgens G, Beeckman T** (2009) Receptor-like kinases shape the plant.  
914 Nature Cell Biology **11**: 1166-1173
- 915 **Deniston CK, Salogiannis J, Mathea S, Snead DM, Lahiri I, Matyszewski M, Donosa O,  
916 Watanabe R, Böhning J, Shiau AK et al.** (2020) Structure of LRRK2 in Parkinson's  
917 disease and model for microtubule interaction. Nature **588**: 344–349

- 918 **Diévarit A, Clark SE** (2004) LRR-containing receptors regulating plant development and  
919 defense. *Development* **131**: 251-261
- 920 **Du D, Liu M, Xing Y, Chen X, Zhang Y, Zhu M, Lu X, Zhang Q, Ling Y, Sang X, Li Y,**  
921 **Zhang C, He G** (2019) Semi-dominant mutation in the cysteine-rich receptor-like kinase  
922 gene, ALS1, conducts constitutive defence response in rice. *Plant Biology* **21**:25-34
- 923 **Du L, Chen Z** (2000) Identification of genes encoding receptor-like protein kinases as  
924 possible targets of pathogen-and salicylic acid-induced WRKY DNA-binding proteins in  
925 Arabidopsis. *Plant Journal* **24**: 837-847
- 926 **Ellis C, Turner JG** (2001) The Arabidopsis mutant *cev1* has constitutively active jasmonate  
927 and ethylene signal pathways and enhanced resistance to pathogens. *Plant Cell* **13**: 1025-1033
- 928 **Ellis C, Karafyllidis I, Wasternack C, Turner JG** (2002) The Arabidopsis Mutant *cev1*  
929 Links Cell Wall Signaling to Jasmonate and Ethylene Responses. *Plant Cell* **14**: 1557-1566
- 930 **Faria-Blanc N, Mortimer JC, Dupree P** (2018) A Transcriptomic Analysis of Xylan  
931 Mutants Does Not Support the Existence of a Secondary Cell Wall Integrity System in  
932 Arabidopsis. *Frontiers in Plant Science* **9**: article 384
- 933 **Friedrichsen DM, Joazeiro CAP, Li J, Hunter T, Chory J** (2000) Brassinosteroid-  
934 Insensitive-1 Is a Ubiquitously Expressed Leucine-Rich Repeat Receptor Serine/Threonine  
935 Kinase. *Plant Physiology* **123**: 1247-1255
- 936 **Hanks SK, Hunter T** (1995) The eukaryotic protein kinase superfamily: kinase (catalytic)  
937 domain structure and classification. *The FASEB Journal* **9**: 576-596
- 938 **Hernández-Blanco C, Feng DX, Hu J, Sanchez-Vallet A, Deslandes L, Llorente F,**  
939 **Berrocal-Lobo M, Keller H, Barlet X, Sanchez-Rodríguez C et al.** (2007) Impairment of  
940 Cellulose Synthases Required for Arabidopsis Secondary Cell Wall Formation Enhances  
941 Disease Resistance. *Plant Cell* **19**: 890–903
- 942 **Houston K, Tucker MR, Chowdhury J, Shirley N, Little A** (2016) The Plant Cell Wall: A  
943 Complex and Dynamic Structure As Revealed by the Responses of Genes under Stress  
944 Conditions. *Frontiers in Plant Science* **7**: article 984
- 945 **Hruz T, Laule O, Szabo G, Wessendorp F, Bleuler S, Oertle L, Widmayer P, Gruissem**  
946 **W, Zimmermann P** (2008) Genevestigator V3: A Reference Expression Database for the  
947 Meta-Analysis of Transcriptomes. *Advances in Bioinformatics* **2008**: article 420747
- 948 **Idänheimo N, Gauthier A, Salojärvi J, Siligato R, Brosché M, Kollist H, Mähönen AP,**  
949 **Kangasjärvi J, Wrzaczek M** (2014) The *Arabidopsis thaliana* cysteine-rich receptor-like

950 kinases CRK6 and CRK7 protect against apoplastic oxidative stress. *Biochemical and*  
951 *Biophysical Research Communications* **445**: 457-462

952 **Janson G, Zhang C, Prado MG, Paiardini A** (2017) PyMod 2.0: improvements in protein  
953 sequence-structure analysis and homology modeling within PyMOL. *Bioinformatics* **33**: 444-  
954 446

955 **Jeffrey PD, Russo AA, Polyak K, Gibbs E, Hurwitz J, Massagé J, Pavletich NP** (1995)  
956 Mechanism of CDK activation revealed by the structure of a cyclinA-CDK2 complex. *Nature*  
957 **376**: 313-320

958 **Kim D, Langmead B, Salzberg SL** (2015) HISAT: a fast spliced aligner with low memory  
959 requirements. *Nature Methods* **12**: 357-360.

960 **Kimura S, Hunter K, Vaahtera L, Tran HC, Citterico M, Vaattovaara A, Rokka A,**  
961 **Stolze SC, Harzen A, Meißner L et al.** (2020) CRK2 and C-terminal phosphorylation of  
962 NADPH oxidase RBOHD regulate reactive oxygen species production in Arabidopsis. *Plant*  
963 *Cell* **32**: 1063-1080

964 **Koornneef M, Reuling G, Karssen CM** (1984) The isolation and characterization of  
965 abscisic acid-insensitive mutants of *Arabidopsis thaliana*. *Physiologia Plantarum* **61**: 377-383

966 **Lefebvre V, Fortabat MN, Ducamp A, North HM, Maia-Grondard A, Trouverie J,**  
967 **Boursiac Y, Mouille G, Durand-Tardif M** (2011) *ESKIMO1* disruption in Arabidopsis  
968 alters vascular tissue and impairs water transport. *PLoS ONE* **6**: e16645

969 **Liao Y, Smyth GK, Shi W** (2019) The R package R subread is easier, faster, cheaper and  
970 better for alignment and quantification of RNA sequencing reads. *Nucleic Acids Research*  
971 **47**: e47

972 **Livak KJ, Schmittgen TD** (2001) Analysis of relative gene expression data using real-time  
973 quantitative PCR and the  $2^{-\Delta\Delta CT}$  method. *Methods* **25**: 402-408

974 **Love MI, Huber W, Anders S** (2014) Moderated estimation of fold change and dispersion  
975 for RNA-seq data with DESeq2. *Genome Biology* **15**: 550.

976 **Ma LS, Wang L, Trippel C, Mendoza-Mendoza A, Ullmann S, Moretti M, Carsten A,**  
977 **Kahnt J, Reissmann S, Zechmann B, Bange G et al.** (2018) The *Ustilago maydis* repetitive  
978 effector Rsp3 blocks the antifungal activity of mannose-binding maize proteins. *Nature*  
979 *Communications* **9**: 1711

- 980 **Masachis S, Segorbe D, Turrà D, Leon-Ruiz M, Fürst U, El Ghalid M, Leonard G,**  
981 **Lopez-Berges MS, Richards TA, Felix G et al.** (2016) A fungal pathogen secretes plant  
982 alkalizing peptides to increase infection. *Nature Microbiology* **1**: 16043
- 983 **Miyakawa T, Miyazono K, Sawano Y, Hatano K, Tanokura M** (2009) Crystal structure of  
984 ginkbilobin-2 with homology to the extracellular domain of plant cysteine-rich receptor-like  
985 kinases. *Proteins* **77**: 247-251
- 986 **Miyakawa T, Hatano K, Miyauchi Y, Suwa Y, Sawano Y, Tanokura M** (2014) A  
987 secreted protein with plant-specific cysteine-rich motif functions as a mannose-binding lectin  
988 that exhibits antifungal activity. *Plant Physiology* **166**: 766-778
- 989 **Molina A, Miedes E, Bacete L, Rodríguez T, Mélida H, Denancé N, Sánchez-Vallet A,**  
990 **Rivière MP, López G, Freydier A et al.** (2021) Arabidopsis cell wall composition  
991 determines disease resistance specificity and fitness. *PNAS* **118**: e2010243118
- 992 **Nolen B, Taylor S, Gourisankar G** (2004) Regulation of Protein Kinases: Controlling  
993 Activity through Activation Segment Conformation. *Molecular Cell* **15**: 661-675
- 994 **Oh MH, Clouse SD, Huber SC** (2012) Tyrosine Phosphorylation of the BRI1 Receptor  
995 Kinase Occurs via a Post-Translational Modification and is Activated by the Juxtamembrane  
996 Domain. *Frontiers in Plant Science* **3**: 175
- 997 **Ohtake Y, Takahashi T, Komeda Y** (2000) Salicylic Acid Induces the Expression of a  
998 Number of Receptor-Like Kinase Genes in *Arabidopsis thaliana*. *Plant & Cell Physiology* **41**:  
999 1038-1044
- 1000 **Oparka K** (1994) Plasmolysis: New Insights into an Old Process. *New Phytologist* **126**: 571-  
1001 591
- 1002 **Perez-Riverol Y, Csordas A, Bai J, Bernal-Llinares M, Hewapathirana S, Kundu DJ,**  
1003 **Inuganti A, Griss J, Mayer G, Eisenacher M et al.** (2019) The PRIDE database and related  
1004 tools and resources in 2019: improving support for quantification data. *Nucleic Acids*  
1005 *Research* **47**: D442-D450
- 1006 **Rajakulendran T, Sahmi M, Lefrançois M, Sicheri F, Therrien M** (2009) A dimerization-  
1007 dependent mechanism drives RAF catalytic activation. *Nature* **461**: 542-545
- 1008 **Reynolds ES** (1963) The use of lead citrate at high pH as an electron-opaque stain in electron  
1009 microscopy. *Journal of Cell Biology* **17**: 208-212.
- 1010 **Seo M, Jikumar Y, Kamiya Y** (2011) Profiling of Hormones and Related Metabolites in  
1011 Seed Dormancy and Germination Studies. *Methods in Molecular Biology* **773**: 99-111.

- 1012 **Shiu SH, Bleecker AB** (2001) Plant Receptor-Like Kinase Gene Family: Diversity,  
1013 Function, and Signaling. *Science Signaling* **2001**: RE22
- 1014 **Sparkes IA, Runions J, Hawes C** (2006) Rapid, transient expression of fluorescent fusion  
1015 proteins in tobacco plants and generation of stably transformed plants. *Nature Protocols* **1**:  
1016 2019-2025
- 1017 **Taylor I, Seitz K, Bennewitz S, Walker JC** (2013) A simple in vitro method to measure  
1018 autophosphorylation of protein kinases. *Plant Methods* **9**: 22
- 1019 **Taylor SS, Kaila-Sharma P, Weng JH, Aoto P, Schmidt SH, Knapp S, Mathea S,**  
1020 **Herberg FW** (2020) Kinase Domain Is a Dynamic Hub for Driving LRRK2 Allostery.  
1021 *Frontiers in Molecular Neuroscience* **13**: 538219
- 1022 **Thomma BPHJ, Eggermont K, Penninckx IAMA, Mauch-Mani B, Vogelsang R,**  
1023 **Cammue BPA, Broekaert WF** (1998) Separate jasmonate-dependent and salicylate-  
1024 dependent defense-response pathways in Arabidopsis are essential for resistance to distinct  
1025 microbial pathogens. *Plant Biology* **95**: 15107-15111
- 1026 **Tian T, Liu Y, Yan H, You Q, Yi X, Du Z, Xu W, Su Z** (2017) agriGO v2.0: a GO analysis  
1027 toolkit for the agricultural community, 2017 update. *Nucleic Acids Research* **45**: W122-  
1028 W129
- 1029 **Turnbull CGN, Booker JP, Leyser HM** (2002) Micrografting techniques for testing long-  
1030 distance signalling in Arabidopsis. *Plant Journal* **32**: 255-262
- 1031 **Turner SR, Somerville CR** (1997) Collapsed Xylem Phenotype of Arabidopsis identifies  
1032 Mutants Deficient in Cellulose Deposition in the Secondary Cell Wall. *The Plant Cell* **9**: 689-  
1033 701
- 1034 **Uknes S, Mauch-Mani B, Moyer M, Potter S, Williams S, Dincher S, Chandler D,**  
1035 **Slusarenko A, Ward E, Ryals J** (1992) Acquired Resistance in Arabidopsis. *The Plant Cell*  
1036 **4**: 645-656
- 1037 **Vaattovaara A, Brandt B, Rajaraman S, Safronov O, Veidenberg A, Luklová M,**  
1038 **Kangasjärvi J, Löytynoja A, Hothorn M, Salojärvi J et al.** (2019) Mechanistic insights  
1039 into the evolution of DUF26-containing proteins in land plants. *Communications Biology*  
1040 **2**:56
- 1041 **Xu D, Dhiman R, Garibay A, Mock HP, Leister D, Kleine T** (2019) Cellulose defects in  
1042 the Arabidopsis secondary cell wall promote early chloroplast development. *Plant Journal*  
1043 **101**: 156-170

1044 **Wang X, Goshe MB, Soderblom EJ, Phinney BS, Kuchar JA, Li J, Asami T, Yoshida S,**  
1045 **Huber SC, Clouse SD** (2005) Identification and functional analysis of in vivo  
1046 phosphorylation sites of the Arabidopsis BRASSINOSTEROID-INSENSITIVE1 receptor  
1047 kinase. *The Plant Cell* **17**: 1685-1703

1048 **Wegener AD, Jones LR** (1984) Phosphorylation-induced mobility shift in phospholambdan  
1049 in sodium dodecyl sulfate-polyacrylamide gels. Evidence for a protein structure consisting of  
1050 multiple identical phosphorylatable subunits. *Journal of Biological Chemistry* **259**: 1834-  
1051 1841

1052 **Wrzaczek M, Brosché M, Salojärvi J, Kangasjärvi S, Idänheimo N, Mersmann S,**  
1053 **Robatzek S, Karpiński S, Karpińska B, Kangasjärvi J** (2010) Transcriptional regulation  
1054 of the CRK/DUF26 group of Receptor-like protein kinases by ozone and plant hormones in  
1055 Arabidopsis. *BMC Plant Biology* **10**: 95

1056 **Yadeta KA, Elmore JM, Creer AY, Feng B, Franco JY, Rufian JS, He P, Phinney B,**  
1057 **Coaker G** (2017) A cysteine-rich protein kinase associates with a membrane immune  
1058 complex and the cysteine residues are required for cell death. *Plant Physiology* **173**: 771-787

1059 **Yan L, Ma Y, Liu D, Wei X, Sun Y, Chen X, Zhao H, Zhou J, Wang Z, Shui W et al.**  
1060 (2012) Structural basis for the impact of phosphorylation on the activation of plant receptor-  
1061 like kinase BAK1. *Cell Research* **22**: 1304-1308

1062 **Yeung W, Ruan Z, Kannan N** (2020) Emerging roles of the  $\alpha$ C- $\beta$ 4 loop in protein kinase  
1063 structure, function, evolution, and disease. *IUBMB Life* **72**: 1189-1202

1064 **Yeh YH, Chang YH, Huang PY, Huang JB, Zimmerli L** (2015) Enhanced Arabidopsis  
1065 pattern-triggered immunity by overexpression of cysteine-rich receptor-like kinases. *Frontiers*  
1066 *in Plant Science* **6**: 1-12

1067 **Zhou Q, Liu J, Wang J, Chen S, Chen L, Wang J, Wang HB, Liu B** (2020) The  
1068 juxtamembrane domains of Arabidopsis CERK1, BAK1, and FLS2 play a conserved role in  
1069 chitin-induced signaling. *Journal of Integrative Plant Biology* **62**: 556-562

1070 **Zipfel C, Kunze G, Chinchilla D, Caniard A, Jones JDG, Boller T, Felix G** (2006)  
1071 Perception of the Bacterial PAMP EF-Tu by the Receptor EFR Restricts Agrobacterium-  
1072 Mediated Transformation. *Cell* **125**: 749-760

1073

1074

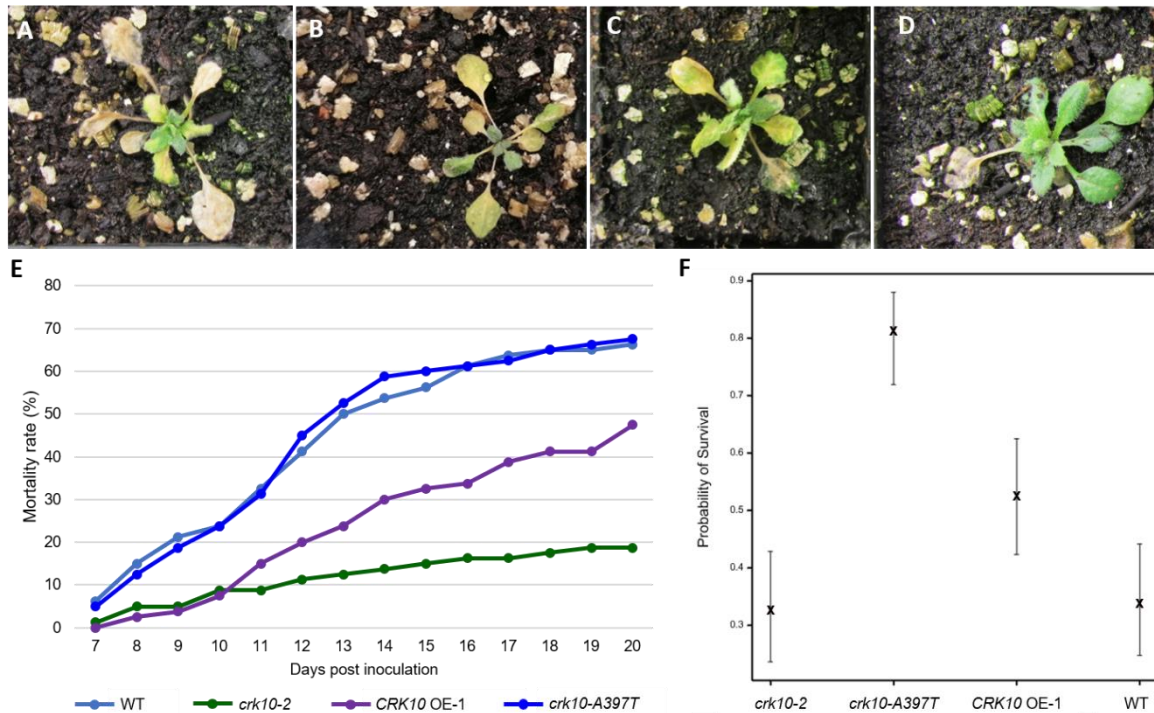


**Figure 7** *crk10-A397T* mutant plants are more resistant to infection with *Fusarium oxysporum* f. sp. *conglutinans* 699. A-D, Representative images of WT (A), *crk10-2* (B), *CRK10* OE-1 (C) and *crk10-A397T* mutant (D) plants at 11 days post inoculation with *F. oxysporum*. E, Mortality curve of WT, *crk10-A397T*, *CRK10* OE-1 and *crk10-2* plants from day 7 to 20 post inoculation with *F. oxysporum*. Mortality is shown in percentage. The experiment was repeated twice with similar results. F, Probability of survival of each genotype following inoculation with the pathogen *F. oxysporum*. Associated 95% confidence intervals are shown. Deviance test,  $\chi^2_3=19.68$ ,  $p < 0.001$ .



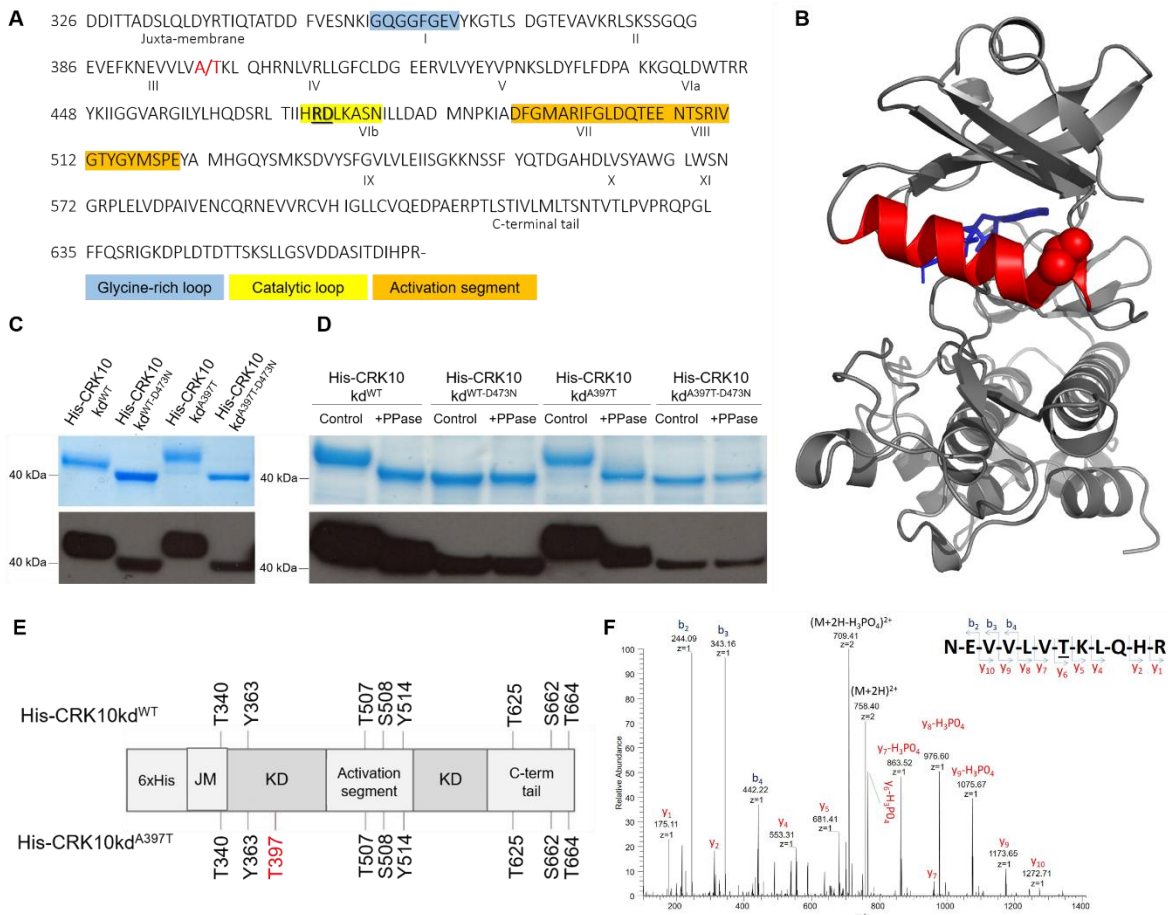


**Figure 1** CRK10 and CRK10-A397 are active kinases and the A397T substitution introduces an additional auto-phosphorylation site in the kinase domain of the protein. A, Amino acid sequence of the cytoplasmic kinase domain of CRK10 used for in situ phosphorylation studies (CRK10 amino acid residue numbering shown on the left). Subdomains I-XI are indicated by roman numerals. Ala/Thr 397 site is highlighted in red, and the RD motif is underlined and highlighted in bold. The conserved glycine-rich loop, catalytic loop and activation segment motifs are also shown. B, Structure of the CRK10 kinase domain generated by homology modelling to the active kinase domain of BRI1. A molecule of an ATP analogue, coloured blue, occupies the active site. The  $\alpha$ -helix is coloured red, and the atoms in the side chain of the mutated threonine residue are depicted as red spheres. C, Recombinant His-CRK10kd<sup>WT</sup> and His-CRK10kd<sup>A397T</sup> extracts and their respective dead kinase controls (His-CRK10kd<sup>WT</sup>-D473N and His-CRK10kd<sup>A397T</sup>-D473N) resolved by SDS-PAGE; detection by Western blot with HRP-conjugated anti-His antibody is shown. D, SDS-PAGE and Western blot following treatment of purified His-tagged proteins with  $\lambda$ -phosphatase (PPase); control: untreated protein. E, In situ auto-phosphorylation sites in His-CRK10kd<sup>WT</sup> and His-CRK10kd<sup>A397T</sup> identified by LC-MS/MS analysis of the recombinant protein kinase domain. Threonine 397 is

highlighted in red. His: 6x His-tag; JM: juxta-membrane domain; KD: kinase domain; C-term tail: C-terminal tail. (f) MS/MS spectrum of the doubly charged ( $m/z$  758.4) tryptic phosphopeptide NEVVLVTKLQHR in which the threonine residue is phosphorylated. Neutral losses of phosphoric acid from both the precursor ion and the C-terminal y ions are observed.

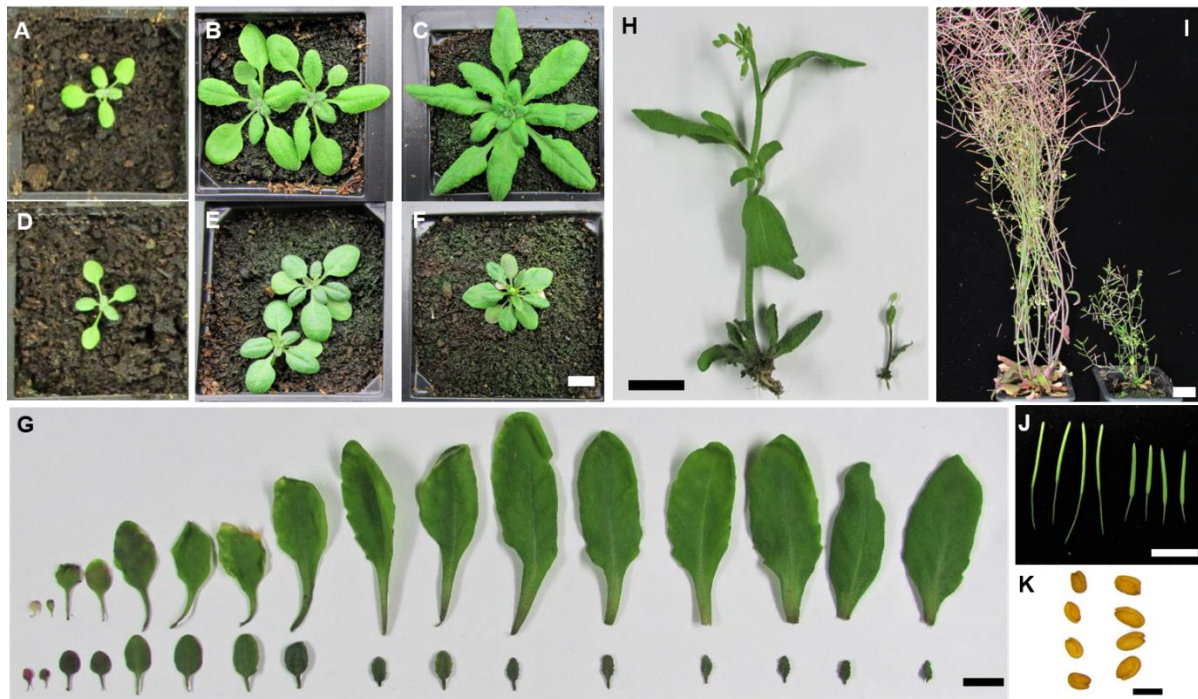


**Figure 2** *crk10-A397T* mutant is a dwarf. A-F, Rosette morphology of WT (A, B, C) and *crk10-A397T* (D, E, F) plants at 2 (A, D), 3 (B, E) and 4 (C, F) weeks after sowing. Bar = 1 cm. G, Leaf series of 4-week-old WT (top) and *crk10-A397T* (bottom) plants. Bar = 1 cm. H, Main inflorescence stem of 5-week-old WT (left) and *crk10-A397T* (right) plants. Bar = 1 cm. I, 10-week-old WT (left) and *crk10-A397T* (right) plants. Bar = 2 cm. J, Siliques of WT (left) and *crk10-A397T* (right) plants. Bar = 1 cm. K, Seeds of WT (left) and *crk10-A397T* (right) plants. Bar = 500 μm.

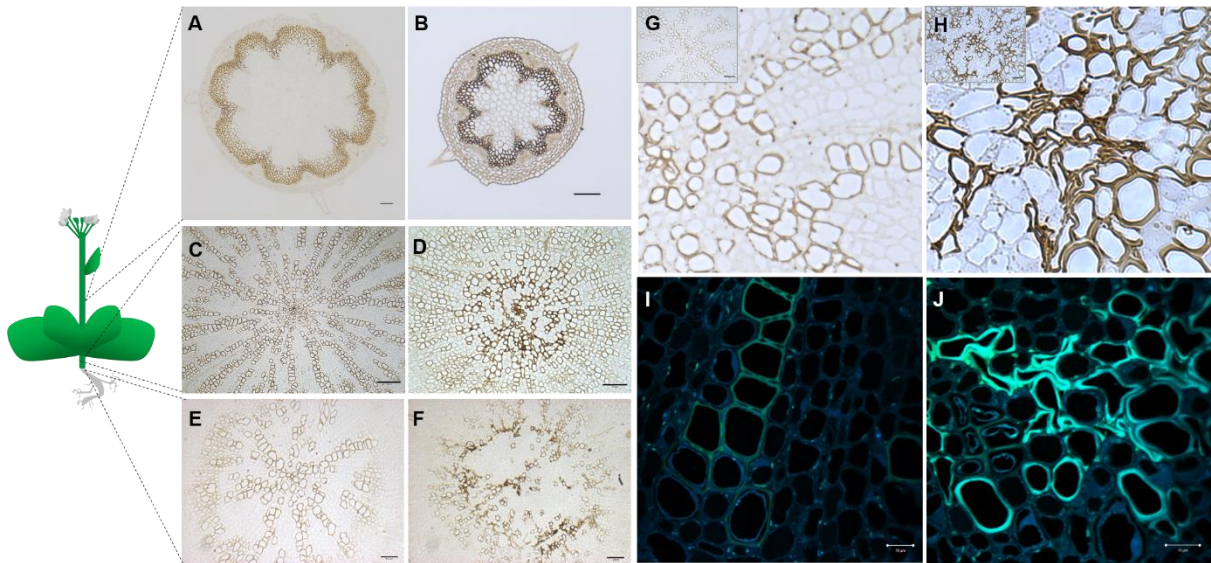


**Figure 3** Xylem vessels collapse in the root and hypocotyl of *crk10-A397T* plants, but not in the stem. A-F, Transverse cross sections of the base of stem (A, B), hypocotyl (C, D) and roots (E, F) of 5-week-old WT (A, C, E) and *crk10-A397T* (B, D, F) plants. Stain: potassium permanganate. Bars = (A, B, C, E, F) 100  $\mu\text{m}$ ; (D) 50  $\mu\text{m}$ . G-H, Detail of xylem vessels in hypocotyls of 4-week-old WT (G) and *crk10-A397T* (H) mutant plants. Stain: potassium permanganate. Insert in top left corner of image shows original micrographs. Bars = (insert G) 50  $\mu\text{m}$ ; (insert H) 25  $\mu\text{m}$ . I-J, Detection of auto-fluorescence of lignin on resin-embedded cross sections of 4-week-old hypocotyls of WT (I) and *crk10-A397T* (J) plants. Bars = 10  $\mu\text{m}$ .

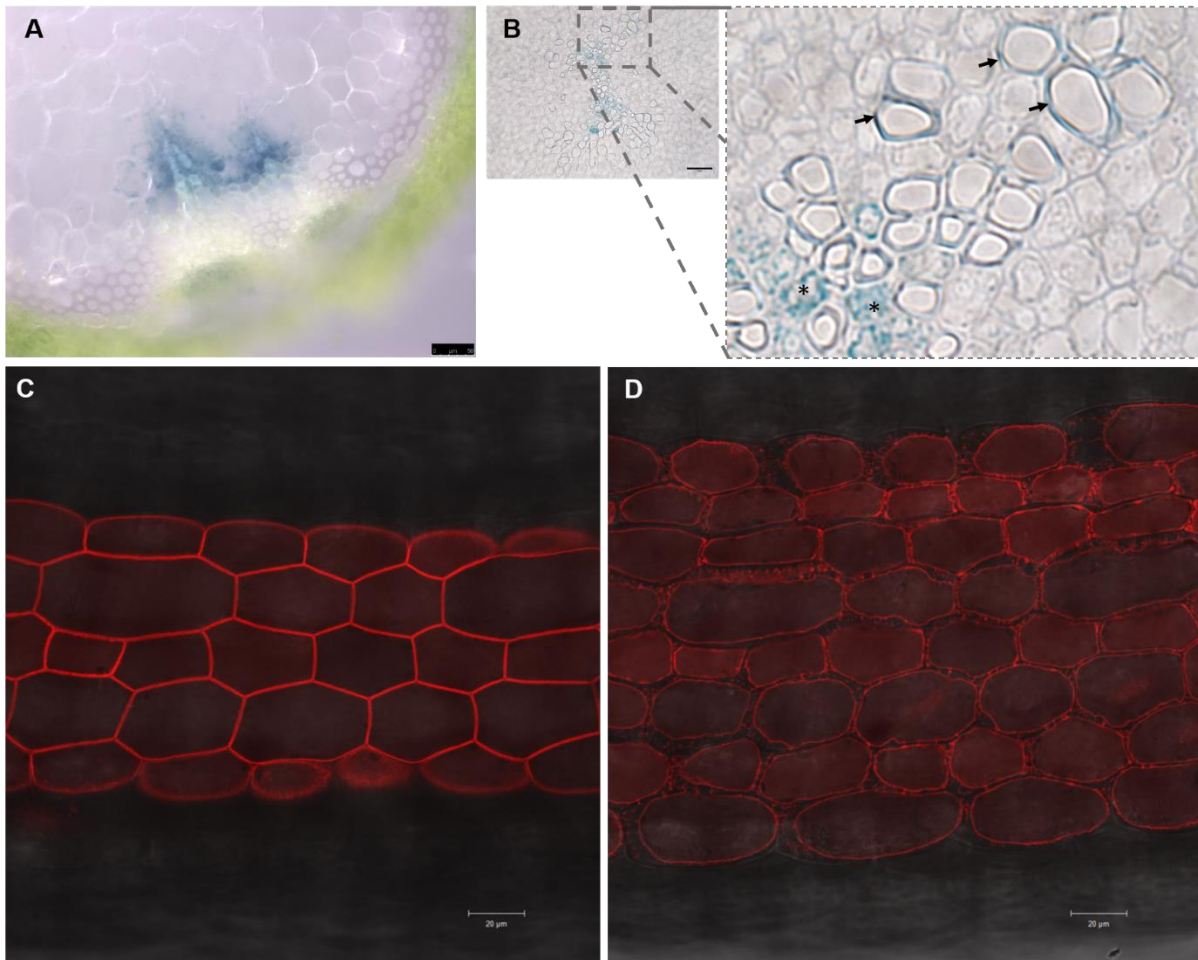


**Figure 4** CRK10 is a plasma membrane-localised protein expressed in association with the vasculature in the hypocotyl. A-B, Histochemical staining of reporter lines expressing the *CRK10*<sub>Pro</sub>:*GUS* construct showed expression of the reporter gene in the vasculature of stem and hypocotyls, as shown by free-hand cross section of 8-week-old inflorescence stem (A) and cross section of 2-week-old hypocotyl embedded in resin (B). Bars = (A) 50  $\mu$ m; (B) 25  $\mu$ m. C, Detail of cross section in B shows presence of histochemical staining in xylem parenchyma cells (asterisks) and differentiating xylem vessels (arrows) in the hypocotyl. C-D, Hypocotyl of 4-day-old seedling of transgenic *Arabidopsis* plant expressing 35S:*CRK10-mCherry* before (C) and after (D) plasmolysis. Bars = 20  $\mu$ m.



**Figure 5** The root-hypocotyl system is responsible for the dwarf phenotype of *crk10-A397T* mutant plants. Images of non-grafted plants (A), self-graft controls (B) and graft combinations (C) of WT and *crk10-A397T* mutant. Plants were imaged 3 weeks after micrografting was performed. The phenotype observed for the reciprocal grafting combinations were consistently observed in two independent repetitions of the experiment. An average number of 10 grafts per combination was recovered each time. Annotation: scion / rootstock.

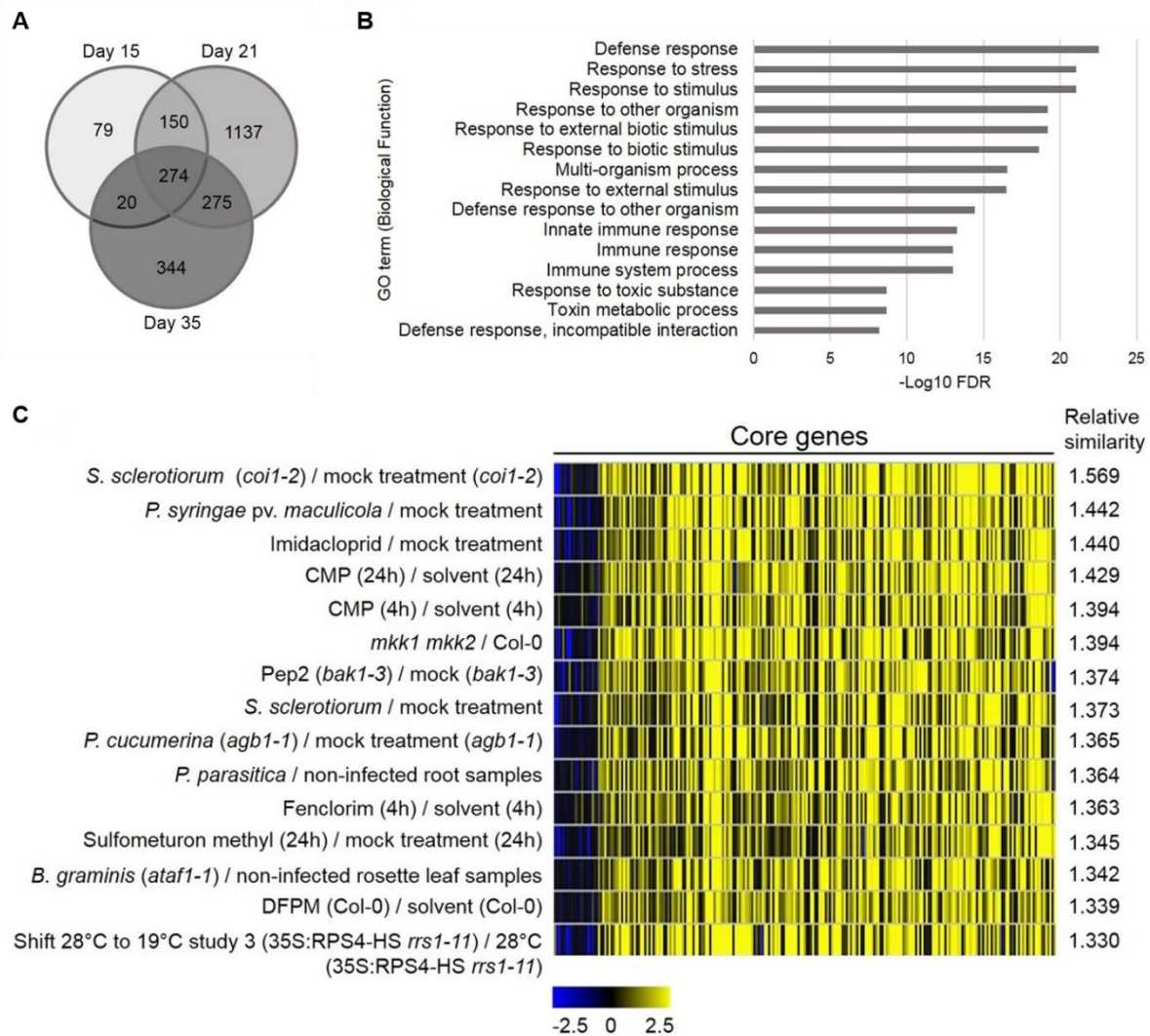


**Figure 6** Transcriptional reprogramming in the *crk10-A397T* mutant shows activation of defense responses to biotic and abiotic stresses. A, Venn diagram displaying the number of differentially expressed genes (DEGs) in the *crk10-A397T* hypocotyls compared to the WT at each developmental time point. B, Top 15 enriched GO terms (Biological Process) for the up-regulated core DEGs in the *crk10-A397T* mutant plotted against their respective  $-\log_{10}$  FDR. C, Top 15 perturbations showing highest overall similarity to *crk10-A397T* mutant expression signature (analysis performed using the GENEVESTIGATOR® SIGNATURE tool;  $\log_2$  fold change values of time point 21 days was used as input for 274 core genes).

## Parsed Citations

Acharya BR, Raina S, Maqbool SB, Jagadeeswaran G, Mosher SL, Appel HM, Schultz JC, Klessig DF, Raina R (2007) Overexpression of CRK13, an Arabidopsis cysteine-rich receptor-like kinase, results in enhanced resistance to Pseudomonas syringae. Plant Journal 50: 488-499

Google Scholar: [Author Only](#) [Title Only](#) [Author and Title](#)

Ahuja I, Kissen R, Bones AM (2012) Phytoalexins in defense against pathogens. Trends in Plant Sciences 17: 73-90

Google Scholar: [Author Only](#) [Title Only](#) [Author and Title](#)

An G, Ebert PR, Mitra A, Ha SB (1988) Binary vectors. In: Gelvin SB, Schilperoot RA eds. Plant Molecular Biology Manual. Kluwer, Dordrecht, Netherlands, A3:1-19

Google Scholar: [Author Only](#) [Title Only](#) [Author and Title](#)

Bacete L, Melida H, Miedes E, Molina A (2018) Plant cell wall-mediated immunity: cell wall changes trigger disease resistance responses. Plant Journal 93: 614-636

Google Scholar: [Author Only](#) [Title Only](#) [Author and Title](#)

Beenstock J, Mooshayef N, Engelberg D (2016) How Do Protein Kinases Take a Selfie (Autophosphorylate)? Trends in Biochemical Sciences 41: 938-953

Google Scholar: [Author Only](#) [Title Only](#) [Author and Title](#)

Bojar D, Martinez J, Santiago J, Rybin V, Bayliss R, Hothorn M (2014) Crystal structures of the phosphorylated BRI1 kinase domain and implications for brassinosteroid signal initiation. Plant Journal 78: 31-43

Google Scholar: [Author Only](#) [Title Only](#) [Author and Title](#)

Bolger AM, Lohse M, Usadel B (2014) Trimmomatic: a flexible trimmer for Illumina sequence data. Bioinformatics 30: 2114-2120

Google Scholar: [Author Only](#) [Title Only](#) [Author and Title](#)

Bourdais G et al. CRK Consortium (2015) Large-Scale Phenomics Identifies Primary and Fine-Tuning Roles for CRKs in Responses Related to Oxidative Stress. PLoS Genetics 11: e1005373

Google Scholar: [Author Only](#) [Title Only](#) [Author and Title](#)

Camut L, Regnault T, Sirlin-Josserand M, Sakvarelidze-Achard L, Carrera E, Zumsteg J, Heintz D, Leonhardt N, Lange MJP, Lange T et al. (2019) Root-derived GA12 contributes to temperature-induced shoot growth in Arabidopsis. Nature Plants 5:1216-1221

Google Scholar: [Author Only](#) [Title Only](#) [Author and Title](#)

Chen Z (2001) A Superfamily of Proteins with Novel Cysteine-Rich Repeats. Plant Physiology 126: 473-476

Google Scholar: [Author Only](#) [Title Only](#) [Author and Title](#)

Chen Z, Hong X, Zhang H, Wang Y, Li X, Zhu JK, Gong Z (2005) Disruption of the cellulose synthase gene, AtCesA8/IRX1, enhances drought and osmotic stress tolerance in Arabidopsis. Plant Journal 43: 273-283

Google Scholar: [Author Only](#) [Title Only](#) [Author and Title](#)

Chinchilla D, Bauer Z, Regenass M, Boller T, Felix G (2006) The Arabidopsis receptor kinase FLS2 binds flg22 and determines the specificity of flagellin perception. Plant Cell 18: 465-476

Google Scholar: [Author Only](#) [Title Only](#) [Author and Title](#)

Clough S, Bent A (1998) Floral dip: A simplified method for Agrobacterium-mediated transformation of Arabidopsis thaliana. Plant Journal 16: 735-743

Google Scholar: [Author Only](#) [Title Only](#) [Author and Title](#)

Czerniec P, Visser B, Sun W, Saviouré A, Deslandes L, Marco Y, Van Montagu M, Verbruggen N (1999) Characterization of an Arabidopsis thaliana receptor-like protein kinase gene activated by oxidative stress and pathogen attack. The Plant Journal 18: 321-327

Google Scholar: [Author Only](#) [Title Only](#) [Author and Title](#)

De Smet I, Voß U, Jürgens G, Beeckman T (2009) Receptor-like kinases shape the plant. Nature Cell Biology 11: 1166-1173

Google Scholar: [Author Only](#) [Title Only](#) [Author and Title](#)

Deniston CK, Salogiannis J, Mathea S, Snead DM, Lahiri I, Matyszewski M, Donosa O, Watanabe R, Böhning J, Shiao AK et al. (2020) Structure of LRRK2 in Parkinson's disease and model for microtubule interaction. Nature 588: 344-349

Google Scholar: [Author Only](#) [Title Only](#) [Author and Title](#)

Diévert A, Clark SE (2004) LRR-containing receptors regulating plant development and defense. Development 131: 251-261

Google Scholar: [Author Only](#) [Title Only](#) [Author and Title](#)

Du D, Liu M, Xing Y, Chen X, Zhang Y, Zhu M, Lu X, Zhang Q, Ling Y, Sang X, Li Y, Zhang C, He G (2019) Semi-dominant mutation in the cysteine-rich receptor-like kinase gene, ALS1, conducts constitutive defence response in rice. Plant Biology 21:25-34

Google Scholar: [Author Only](#) [Title Only](#) [Author and Title](#)

Du L, Chen Z (2000) Identification of genes encoding receptor-like protein kinases as possible targets of pathogen-and salicylic acid-induced WRKY DNA-binding proteins in Arabidopsis. Plant Journal 24: 837-847

Google Scholar: [Author Only](#) [Title Only](#) [Author and Title](#)

**Ellis C, Turner JG (2001) The Arabidopsis mutant cev1 has constitutively active jasmonate and ethylene signal pathways and enhanced resistance to pathogens. Plant Cell 13: 1025-1033**

Google Scholar: [Author Only](#) [Title Only](#) [Author and Title](#)

**Ellis C, Karafyllidis I, Wasternack C, Turner JG (2002) The Arabidopsis Mutant cev1 Links Cell Wall Signaling to Jasmonate and Ethylene Responses. Plant Cell 14: 1557-1566**

Google Scholar: [Author Only](#) [Title Only](#) [Author and Title](#)

**Faria-Blanc N, Mortimer JC, Dupree P (2018) A Transcriptomic Analysis of Xylan Mutants Does Not Support the Existence of a Secondary Cell Wall Integrity System in Arabidopsis. Frontiers in Plant Science 9: article 384**

Google Scholar: [Author Only](#) [Title Only](#) [Author and Title](#)

**Friedrichsen DM, Joazeiro CAP, Li J, Hunter T, Chory J (2000) Brassinosteroid-Insensitive-1 Is a Ubiquitously Expressed Leucine-Rich Repeat Receptor Serine/Threonine Kinase. Plant Physiology 123: 1247-1255**

Google Scholar: [Author Only](#) [Title Only](#) [Author and Title](#)

**Hanks SK, Hunter T (1995) The eukaryotic protein kinase superfamily: kinase (catalytic) domain structure and classification. The FASEB Journal 9: 576-596**

Google Scholar: [Author Only](#) [Title Only](#) [Author and Title](#)

**Hernández-Blanco C, Feng DX, Hu J, Sanchez-Vallet A, Deslandes L, Llorente F, Berrocal-Lobo M, Keller H, Barlet X, Sanchez-Rodríguez C et al. (2007) Impairment of Cellulose Synthases Required for Arabidopsis Secondary Cell Wall Formation Enhances Disease Resistance. Plant Cell 19: 890-903**

Google Scholar: [Author Only](#) [Title Only](#) [Author and Title](#)

**Houston K, Tucker MR, Chowdhury J, Shirley N, Little A (2016) The Plant Cell Wall: A Complex and Dynamic Structure As Revealed by the Responses of Genes under Stress Conditions. Frontiers in Plant Science 7: article 984**

Google Scholar: [Author Only](#) [Title Only](#) [Author and Title](#)

**Hruz T, Laule O, Szabo G, Wessendorp F, Bleuler S, Oertle L, Widmayer P, Gruissem W, Zimmermann P (2008) Genevestigator V3: A Reference Expression Database for the Meta-Analysis of Transcriptomes. Advances in Bioinformatics 2008: article 420747**

Google Scholar: [Author Only](#) [Title Only](#) [Author and Title](#)

**Idänheimo N, Gauthier A, Salojärvi J, Siligato R, Brosché M, Kollist H, Mähönen AP, Kangasjärvi J, Wrzaczek M (2014) The Arabidopsis thaliana cysteine-rich receptor-like kinases CRK6 and CRK7 protect against apoplastic oxidative stress. Biochemical and Biophysical Research Communications 445: 457-462**

Google Scholar: [Author Only](#) [Title Only](#) [Author and Title](#)

**Janson G, Zhang C, Prado MG, Paiardini A (2017) PyMod 2.0: improvements in protein sequence-structure analysis and homology modeling within PyMOL. Bioinformatics 33: 444-446**

Google Scholar: [Author Only](#) [Title Only](#) [Author and Title](#)

**Jeffrey PD, Russo AA, Polyak K, Gibbs E, Hurwitz J, Massagé J, Pavletich NP (1995) Mechanism of CDK activation revealed by the structure of a cyclinA-CDK2 complex. Nature 376: 313-320**

Google Scholar: [Author Only](#) [Title Only](#) [Author and Title](#)

**Kim D, Langmead B, Salzberg SL (2015) HISAT: a fast spliced aligner with low memory requirements. Nature Methods 12: 357-360.**

Google Scholar: [Author Only](#) [Title Only](#) [Author and Title](#)

**Kimura S, Hunter K, Vaahtera L, Tran HC, Citterico M, Vaattovaara A, Rokka A, Stolze SC, Harzen A, Meißner L et al. (2020) CRK2 and C-terminal phosphorylation of NADPH oxidase RBOHD regulate reactive oxygen species production in Arabidopsis. Plant Cell 32: 1063-1080**

Google Scholar: [Author Only](#) [Title Only](#) [Author and Title](#)

**Koornneef M, Reuling G, Karssen CM (1984) The isolation and characterization of abscisic acid-insensitive mutants of Arabidopsis thaliana. Physiologia Plantarum 61: 377-383**

Google Scholar: [Author Only](#) [Title Only](#) [Author and Title](#)

**Lefebvre V, Fortabat MN, Ducamp A, North HM, Maia-Grondard A, Trouverie J, Boursiac Y, Mouille G, Durand-Tardif M (2011) ESKIMO1 disruption in Arabidopsis alters vascular tissue and impairs water transport. PLoS ONE 6: e16645**

Google Scholar: [Author Only](#) [Title Only](#) [Author and Title](#)

**Liao Y, Smyth GK, Shi W (2019) The R package R subread is easier, faster, cheaper and better for alignment and quantification of RNA sequencing reads. Nucleic Acids Research 47: e47**

Google Scholar: [Author Only](#) [Title Only](#) [Author and Title](#)

**Livak KJ, Schmittgen TD (2001) Analysis of relative gene expression data using real-time quantitative PCR and the 2- $\Delta\Delta$ CT method. Methods 25: 402-408**

Google Scholar: [Author Only](#) [Title Only](#) [Author and Title](#)

**Love MI, Huber W, Anders S (2014) Moderated estimation of fold change and dispersion for RNA-seq data with DESeq2. Genome Biology 15: 550.**

- Google Scholar: [Author Only](#) [Title Only](#) [Author and Title](#)
- Ma LS, Wang L, Trippel C, Mendoza-Mendoza A, Ullmann S, Moretti M, Carsten A, Kahnt J, Reissmann S, Zechmann B, Bange G et al. (2018) The *Ustilago maydis* repetitive effector Rsp3 blocks the antifungal activity of mannose-binding maize proteins. *Nature Communications* 9: 1711**  
Google Scholar: [Author Only](#) [Title Only](#) [Author and Title](#)
- Masachis S, Segorbe D, Turrà D, Leon-Ruiz M, Fürst U, El Ghalid M, Leonard G, Lopez-Berges MS, Richards TA, Felix G et al. (2016) A fungal pathogen secretes plant alkalizing peptides to increase infection. *Nature Microbiology* 1: 16043**  
Google Scholar: [Author Only](#) [Title Only](#) [Author and Title](#)
- Miyakawa T, Miyazono K, Sawano Y, Hatano K, Tanokura M (2009) Crystal structure of ginkbilobin-2 with homology to the extracellular domain of plant cysteine-rich receptor-like kinases. *Proteins* 77: 247-251**  
Google Scholar: [Author Only](#) [Title Only](#) [Author and Title](#)
- Miyakawa T, Hatano K, Miyauchi Y, Suwa Y, Sawano Y, Tanokura M (2014) A secreted protein with plant-specific cysteine-rich motif functions as a mannose-binding lectin that exhibits antifungal activity. *Plant Physiology* 166: 766-778**  
Google Scholar: [Author Only](#) [Title Only](#) [Author and Title](#)
- Molina A, Miedes E, Bacete L, Rodríguez T, Mérida H, Denancé N, Sánchez-Vallet A, Rivière MP, López G, Freyrier A et al. (2021) *Arabidopsis* cell wall composition determines disease resistance specificity and fitness. *PNAS* 118: e2010243118**  
Google Scholar: [Author Only](#) [Title Only](#) [Author and Title](#)
- Nolen B, Taylor S, Gourisankar G (2004) Regulation of Protein Kinases: Controlling Activity through Activation Segment Conformation. *Molecular Cell* 15: 661-675**  
Google Scholar: [Author Only](#) [Title Only](#) [Author and Title](#)
- Oh MH, Clouse SD, Huber SC (2012) Tyrosine Phosphorylation of the BRI1 Receptor Kinase Occurs via a Post-Translational Modification and is Activated by the Juxtamembrane Domain. *Frontiers in Plant Science* 3: 175**  
Google Scholar: [Author Only](#) [Title Only](#) [Author and Title](#)
- Ohtake Y, Takahashi T, Komeda Y (2000) Salicylic Acid Induces the Expression of a Number of Receptor-Like Kinase Genes in *Arabidopsis thaliana*. *Plant & Cell Physiology* 41: 1038-1044**  
Google Scholar: [Author Only](#) [Title Only](#) [Author and Title](#)
- Oparka K (1994) Plasmolysis: New Insights into an Old Process. *New Phytologist* 126: 571-591**  
Google Scholar: [Author Only](#) [Title Only](#) [Author and Title](#)
- Perez-Riverol Y, Csordas A, Bai J, Bernal-Llinares M, Hewapathirana S, Kundu DJ, Inuganti A, Griss J, Mayer G, Eisenacher M et al. (2019) The PRIDE database and related tools and resources in 2019: improving support for quantification data. *Nucleic Acids Research* 47: D442-D450**  
Google Scholar: [Author Only](#) [Title Only](#) [Author and Title](#)
- Rajakulendran T, Sahmi M, Lefrançois M, Sicheri F, Therrien M (2009) A dimerization-dependent mechanism drives RAF catalytic activation. *Nature* 461: 542-545**  
Google Scholar: [Author Only](#) [Title Only](#) [Author and Title](#)
- Reynolds ES (1963) The use of lead citrate at high pH as an electron-opaque stain in electron microscopy. *Journal of Cell Biology* 17: 208-212.**  
Google Scholar: [Author Only](#) [Title Only](#) [Author and Title](#)
- Seo M, Jikumaru Y, Kamiya Y (2011) Profiling of Hormones and Related Metabolites in Seed Dormancy and Germination Studies. *Methods in Molecular Biology* 773: 99-111.**  
Google Scholar: [Author Only](#) [Title Only](#) [Author and Title](#)
- Shiu SH, Bleecker AB (2001) Plant Receptor-Like Kinase Gene Family: Diversity, Function, and Signaling. *Science Signaling* 2001: RE22**  
Google Scholar: [Author Only](#) [Title Only](#) [Author and Title](#)
- Sparkes IA, Runions J, Hawes C (2006) Rapid, transient expression of fluorescent fusion proteins in tobacco plants and generation of stably transformed plants. *Nature Protocols* 1: 2019-2025**  
Google Scholar: [Author Only](#) [Title Only](#) [Author and Title](#)
- Taylor I, Seitz K, Bennewitz S, Walker JC (2013) A simple in vitro method to measure autophosphorylation of protein kinases. *Plant Methods* 9: 22**  
Google Scholar: [Author Only](#) [Title Only](#) [Author and Title](#)
- Taylor SS, Kaila-Sharma P, Weng JH, Aoto P, Schmidt SH, Knapp S, Mathea S, Herberg FW (2020) Kinase Domain Is a Dynamic Hub for Driving LRRK2 Allostery. *Frontiers in Molecular Neuroscience* 13: 538219**  
Google Scholar: [Author Only](#) [Title Only](#) [Author and Title](#)
- Thomma BPHJ, Eggermont K, Penninckx IAMA, Mauch-Mani B, Vogelsang R, Cammue BPA, Broekaert WF (1998) Separate jasmonate-dependent and salicylate-dependent defense-response pathways in *Arabidopsis* are essential for resistance to distinct microbial pathogens. *Plant Biology* 95: 15107-15111**

Google Scholar: [Author Only](#) [Title Only](#) [Author and Title](#)

Tian T, Liu Y, Yan H, You Q, Yi X, Du Z, Xu W, Su Z (2017) agriGO v2.0: a GO analysis toolkit for the agricultural community, 2017 update. *Nucleic Acids Research* 45: W122-W129

Google Scholar: [Author Only](#) [Title Only](#) [Author and Title](#)

Turnbull CGN, Booker JP, Leyser HM (2002) Micrografting techniques for testing long-distance signalling in *Arabidopsis*. *Plant Journal* 32: 255-262

Google Scholar: [Author Only](#) [Title Only](#) [Author and Title](#)

Turner SR, Somerville CR (1997) Collapsed Xylem Phenotype of *Arabidopsis* identifies Mutants Deficient in Cellulose Deposition in the Secondary Cell Wall. *The Plant Cell* 9: 689-701

Google Scholar: [Author Only](#) [Title Only](#) [Author and Title](#)

Uknes S, Mauch-Mani B, Moyer M, Potter S, Williams S, Dincher S, Chandler D, Slusarenko A, Ward E, Ryals J (1992) Acquired Resistance in *Arabidopsis*. *The Plant Cell* 4: 645-656

Google Scholar: [Author Only](#) [Title Only](#) [Author and Title](#)

Vaattovaara A, Brandt B, Rajaraman S, Safronov O, Veidenberg A, Luklová M, Kangasjärvi J, Löytynoja A, Hothorn M, Salojärvi J et al. (2019) Mechanistic insights into the evolution of DUF26-containing proteins in land plants. *Communications Biology* 2:56

Google Scholar: [Author Only](#) [Title Only](#) [Author and Title](#)

Xu D, Dhiman R, Garibay A, Mock HP, Leister D, Kleine T (2019) Cellulose defects in the *Arabidopsis* secondary cell wall promote early chloroplast development. *Plant Journal* 101: 156-170

Google Scholar: [Author Only](#) [Title Only](#) [Author and Title](#)

Wang X, Goshe MB, Soderblom EJ, Phinney BS, Kuchar JA, Li J, Asami T, Yoshida S, Huber SC, Clouse SD (2005) Identification and functional analysis of in vivo phosphorylation sites of the *Arabidopsis* BRASSINOSTEROID-INSENSITIVE1 receptor kinase. *The Plant Cell* 17: 1685-1703

Google Scholar: [Author Only](#) [Title Only](#) [Author and Title](#)

Wegener AD, Jones LR (1984) Phosphorylation-induced mobility shift in phospholamban in sodium dodecyl sulfate-polyacrylamide gels. Evidence for a protein structure consisting of multiple identical phosphorylatable subunits. *Journal of Biological Chemistry* 259: 1834-1841

Google Scholar: [Author Only](#) [Title Only](#) [Author and Title](#)

Wrzaczek M, Brosché M, Salojärvi J, Kangasjärvi S, Idänheimo N, Mersmann S, Robatzek S, Karpiński S, Karpińska B, Kangasjärvi J (2010) Transcriptional regulation of the CRK/DUF26 group of Receptor-like protein kinases by ozone and plant hormones in *Arabidopsis*. *BMC Plant Biology* 10: 95

Google Scholar: [Author Only](#) [Title Only](#) [Author and Title](#)

Yadeta KA, Elmore JM, Creer AY, Feng B, Franco JY, Rufian JS, He P, Phinney B, Coaker G (2017) A cysteine-rich protein kinase associates with a membrane immune complex and the cysteine residues are required for cell death. *Plant Physiology* 173: 771-787

Google Scholar: [Author Only](#) [Title Only](#) [Author and Title](#)

Yan L, Ma Y, Liu D, Wei X, Sun Y, Chen X, Zhao H, Zhou J, Wang Z, Shui W et al. (2012) Structural basis for the impact of phosphorylation on the activation of plant receptor-like kinase BAK1. *Cell Research* 22: 1304-1308

Google Scholar: [Author Only](#) [Title Only](#) [Author and Title](#)

Yeung W, Ruan Z, Kannan N (2020) Emerging roles of the  $\alpha$ C- $\beta$ 4 loop in protein kinase structure, function, evolution, and disease. *IUBMB Life* 72: 1189-1202

Google Scholar: [Author Only](#) [Title Only](#) [Author and Title](#)

Yeh YH, Chang YH, Huang PY, Huang JB, Zimmerli L (2015) Enhanced *Arabidopsis* pattern-triggered immunity by overexpression of cysteine-rich receptor-like kinases. *Frontiers in Plant Science* 6: 1-12

Google Scholar: [Author Only](#) [Title Only](#) [Author and Title](#)

Zhou Q, Liu J, Wang J, Chen S, Chen L, Wang J, Wang HB, Liu B (2020) The juxtamembrane domains of *Arabidopsis* CERK1, BAK1, and FLS2 play a conserved role in chitin-induced signaling. *Journal of Integrative Plant Biology* 62: 556-562

Google Scholar: [Author Only](#) [Title Only](#) [Author and Title](#)

Zipfel C, Kunze G, Chinchilla D, Caniard A, Jones JDG, Boller T, Felix G (2006) Perception of the Bacterial PAMP EF-Tu by the Receptor EFR Restricts *Agrobacterium*-Mediated Transformation. *Cell* 125: 749-760

Google Scholar: [Author Only](#) [Title Only](#) [Author and Title](#)